Integrative analysis of pre-treatment RNA expression signatures and recurrent genomic alterations: Short-term endocrine therapy response and disease-free survival in luminal breast cancer

Guokun Zhang[1], Hua Ni[2], Lidiya Mishieva[3,4], Stephan Bartels[5], Matthias Christgen[5], Henriette Christgen[5], Leonie Donata Kandt[5], Mieke Raap[5], Ronald E. Kates[6], Oleg Gluz[6,7,8], Monika Graeser[6,7,9], Sherko Kümmel[6,10,11], Ulrike Nitz[6,7], Christoph Plass[12], Ulrich Mansmann[1], Christine zu Eulenburg[6,13], Clarissa Gerhäuser[12*], Hans H. Kreipe[5,6], Nadia Harbeck[2,6]

[1]Institute for Medical Information Processing, Biometry, and Epidemiology, Medical Faculty, Ludwig Maximilians University (LMU), Munich, Germany

[2]Breast Center, Department OB&GYN and CCC Munich, LMU University Hospital, Munich, Germany

[3]Institute of Sociology (IfS), Faculty of Social Sciences, University of Bremen, Bremen, Germany

[4]Department of Methodology and Statistics, Faculty of Social & Behavioural Sciences, Utrecht University, Utrecht, The Netherlands

[5]Institute of Pathology, Hannover Medical School, Hannover, Germany

[6]West German Study Group (WSG), Moenchengladbach, Germany

[7]Ev. Bethesda Hospital, Breast Center Niederrhein, Moenchengladbach, Germany

[8]University Clinics Cologne, Women's Clinic and Breast Center, Cologne, Germany

[9]Department of Gynecology, University Medical Center Hamburg, Germany

[10]Clinics Essen-Mitte, Breast Unit, Essen, Germany

[11]Charité - Universitätsmedizin Berlin, Department of Gynecology with Breast Center, Berlin, Germany

[12]Division of Cancer Epigenomics, German Cancer Research Center (DKFZ), Heidelberg, Germany

[13]Department of Biometry and Epidemiology, University Medical Center Hamburg, Hamburg, Germany

Present address HN: Department of Pathology, School of Basic Medical Sciences, Peking University Third Hospital, Peking University Health Science Center

*Corresponding author:

Dr. Clarissa Gerhäuser, Division of Cancer Epigenomics, German Cancer Research Center, Im Neuenheimer Feld 280, 69120 Heidelberg, Germany

Phone: +40 6221 423306, email: c.gerhauser@dkfz.de

Abstract

Background

Endocrine therapy with tamoxifen or aromatase inhibitors is an effective treatment in patients with estrogen receptor-positive, HER2-negative luminal breast cancer. However, many patients do not respond to this therapy, leading to disease recurrence. This study aimed to identify baseline clinical, molecular, and genetic features associated with endocrine therapy response and long-term outcomes in luminal breast cancer.

Methods

We analyzed 220 patients from the WSG-ADAPT trial with early-stage, estrogen receptor-positive, HER2-negative breast cancer, who received three weeks of preoperative endocrine therapy with tamoxifen or an aromatase inhibitor. Short-term treatment response was assessed by immunohistochemical labeling of proliferating cells with baseline Ki67. Pre-treatment tumor samples were profiled using the NanoString BC360 panel, measuring mRNA expression of 758 genes grouped into 42 biological signatures. Post-treatment samples were analyzed for recurrent genomic alterations. Long-term outcome was assessed by invasive- and distant disease-free survival in 191 patients, with a median follow-up time of 59.8 months. Statistical methods in this exploratory approach included mixed-effects modeling, correlation analysis, differential expression testing and survival analysis.

Results

Baseline clinical factors such as patient age, tumor subtype, and immune infiltration were associated with treatment response. Non-responders more frequently harbored *TP53* mutations and *CCND1* amplifications, which were linked to significantly elevated expression of immune- (APM, IFN-γ, Treg) and proliferation-related signatures (BC

Proliferation, Genomic Risk, HRD), particularly in the tamoxifen-treated group. When we stratified the cohort by Oncotype DX recurrence scores (RS), additional signatures such as Mast cells and Mammary Stemness were found significantly upregulated in younger RS2 cases (age ≤ 51 years) not responding to endocrine therapy. In the aromatase inhibitor-treated group, signatures associated with reduced invasive or distant disease-free survival included BC p53 (hazard ratio (HR) with 95% confidence interval (CI) = 2.74 [1.08-6.94]), Genomic Risk (2.5 [1.07-5.83]), HRD (2.44 [1.12-5.29]), ERBB2 (2.46 [1.05-5.75]) and Hypoxia (2.12 [1.17-3.87]), while high expression of PD-1 indicated better outcomes (0.44 [0.21-0.94]).

Conclusions

Endocrine resistance in luminal breast cancer involves elevated immune signatures, increased proliferation, and specific genomic alterations. Combining clinical information, gene expression, and genetic data improves patient stratification and may inform treatment decisions. These findings support the use of integrative analyses to guide personalized endocrine therapy and improve outcomes.

Trial registration: WSG-ADAPT, NCT01779206, Registered 2013-01-25, retrospectively registered.

Keywords

luminal breast cancer, endocrine therapy, primary resistance, gene expression signatures, NanoString BC360, recurrent genomic alterations, disease-free survival

Background

Estrogen receptor-positive (ER+) breast cancer accounts for approximately 75% of breast cancer diagnoses and relies primarily on estrogen signaling for tumor growth and progression [1]. Standard treatments for ER+ breast cancer involve endocrine

therapies, including selective estrogen receptor modulators such as tamoxifen (TAM), and aromatase inhibitors (AI), which inhibit estrogen production [2]. Although initially effective, endocrine resistance represents a significant clinical challenge, as up to 40% of patients experience disease relapse during or after endocrine therapy [3]. Understanding the mechanisms underlying endocrine resistance is therefore essential to improve patient prognosis and inform treatment decisions.

Endocrine resistance in ER+ breast cancer is broadly categorized into primary resistance, where tumors fail to respond to initial hormone therapy, and secondary resistance, which emerges after an initial period of responsiveness [4,5]. This study focuses on primary resistance, which is determined by tumor-intrinsic and microenvironmental factors present before the start of endocrine therapy.

The West German Study Group Adjuvant Dynamic marker-Adjusted Personalized Therapy (WSG-ADAPT) trial, which has enrolled more than 5600 patients with luminal BC to date, provides a novel approach to investigating endocrine resistance [6]. This trial includes 2290 early-stage, ER-positive, HER2-negative breast cancer patients who received a short (3-week) course of preoperative endocrine therapy (pET) prior to surgery. Treatment response is assessed using Ki67 immunohistochemistry as a marker of tumor proliferation before and after pET. Based on changes in Ki67 levels, patients are classified as responders or non-responders. This design offers a unique opportunity to investigate pre-treatment baseline tumor biology and gene expression in relation to short-term endocrine response.

Growing evidence highlights the value of integrative transcriptomic approaches in uncovering biological pathways associated with primary endocrine resistance. An early study investigating array-based gene expression of 15 patients (pre- and post-treatment), who participated in a randomized Phase II clinical trial of 4 months of

neoadjuvant endocrine therapy, identified aberrant estrogen signaling as a key feature associated with intrinsic resistance [7]. Goto-Yamaguchi et al. performed RT-PCR-based mRNA-expression analyses of 40 pre-selected genes in pre-treatment samples from 78 ER+ breast cancer cases receiving short- (2-8 weeks; n = 37) or long-term (over 4 months; n = 40) neoadjuvant endocrine therapy. The study suggested that therapy response may be linked to a hypoxic tumor microenvironment and immune activation [8]. Collectively, these studies suggest that primary endocrine resistance is associated with distinct gene expression programs and molecular features that can be detected at baseline, supporting the development of integrated biomarker strategies to inform early treatment decisions in ER+ breast cancer.

The NanoString Breast Cancer 360 (BC360) panel analyzes the expression of 758 curated genes relevant to breast cancer biology, stratified into 42 NanoString signatures, which reflect tumor-intrinsic processes, immune activity, tumor microenvironment composition, and key breast cancer pathways [9]. These signatures provide an opportunity to explore not only prognostic risk but also predictive markers of endocrine responsiveness. The advantages of the NanoString technology are small sample requirements and the usability of RNA extracted from formalin-fixed biopsy material.

The Oncotype DX Recurrence Score (RS) estimates the risk of distant recurrence based on the mRNA expression of 21 genes [10] and is widely used in the clinics to guide treatment decisions, particularly regarding the need for adjuvant chemotherapy in ER+ breast cancer patients [11]. Based on the RS, patients are categorized into low-, intermediate-, and high-risk groups, enabling a more individualized approach to treatment.

By integrating comprehensive transcriptomic profiling from the BC360 panel with information on therapy response, RS groupings, clinical and genomic data, our study aimed to identify molecular signatures associated with endocrine resistance and to uncover potential mechanisms. These findings may inform strategies for personalized therapy in ER+ breast cancer.

Methods

Patient cohort

This study analyzed a subset (n = 220) of early-stage breast cancer patients enrolled in the phase II WSG-ADAPT trial (NCT01779206) as described earlier [12]. Eligible patients had ER+ and/or PR+, HER2- tumors and received three weeks of preoperative endocrine therapy (pET): tamoxifen (TAM) for premenopausal and aromatase inhibitors (AI) for postmenopausal patients (clinicopathological characteristics summarized in Supplementary Table S1). Formalin-fixed, paraffin-embedded (FFPE) tumor biopsies were collected at baseline and post-pET. Endocrine response was evaluated based on post-pET Ki67 staining and its change from baseline. Responders (R) were stringently defined by post-pET Ki67 < 10% and a ≥ 70% decrease from baseline. Non-responders (NR) had post-pET Ki67 ≥ 20% and a ≤ 20% decrease. R and NR patients were partially matched for histopathologic features at baseline, including histologic grade, pT, pN, ER, PR, HER2 status and oncotype DX Recurrence Score (RS). The cohort is a subset of the discovery cohort with a matched pair design as described in Ref. [12]. The matched pair design was partially broken since RNA was not available for all cases (pairing information in Supplementary Table S2 Tab2). Stromal tumor-infiltrating lymphocytes (TILs) were assessed on baseline FFPE tumor specimens. The TILs score was defined as the

percentage of stromal area infiltrated by lymphocytes, ranging from 0% to 100%. For statistical analyses, TILs scores were also grouped into three categories: Group 1 (0–9%), Group 2 (10–40%), and Group 3 (41–100%). Additional clinicopathologic data and matching strategy are detailed as described in Ref. [12].

NanoString gene expression profiling

Gene expression profiling was performed using the NanoString Breast Cancer 360™ (BC360) panel, which includes 758 genes grouped into 42 signatures across four biological categories: Tumor Intrinsic, Immune Response, Microenvironment, and Breast Cancer–related pathways (Supplementary Table S2 Tab3). Genes comprising the RNA expression signatures measured with the BC360 panel are described in Ref. [13].

RNA was extracted from FFPE tumor biopsies collected at diagnosis, before endocrine therapy was initiated. NanoString profiling followed the manufacturer's protocol and was performed in three main steps: (1) hybridization of RNA with CodeSet probes, (2) purification and immobilization using the nCounter® Prep Station, and (3) digital counting of barcode-labeled probes on the nCounter® Analyzer. The BC360 panel version NS_BC_360_V2.0 was used with high sensitivity settings. Raw count data were saved as RCC files and imported into nSolver 4.0 for data quality control and normalization. During quality control, samples with irregular control probe distributions were excluded. Normalization was performed by NanoString using their in-house pipeline. PAM50 molecular subtypes were assigned by correlating expression values to established subtype centroids, and the subtype with the highest correlation was used as the classification [14]. Genomic Risk scores were calculated from PAM50 and proliferation gene expression signatures and scaled from 0 to 100. Tumor size was

not included in the score calculation, consistent with standard genomic-only methods [9].

Correlation of NanoString signatures

Spearman correlation coefficients were calculated between baseline NanoString BC360 signature scores, selected clinicopathological features, RS group information, NanoString PAM50 subtype correlations and our recently developed Predictive Endocrine ResistanCe Index (PERCI) [12]. Analyses were performed separately for the TAM and AI cohorts. *P*-values were adjusted using the Benjamini-Hochberg false discovery rate (FDR) correction, and only correlations with FDR < 0.01 were considered statistically significant. Significant correlations were visualized using correlation plots (R package corrplot version: 0.92). Hierarchical clustering of signatures was performed using ward.D2 linkage. Major clusters were grouped into blocks of signatures with high positive correlation of expression. Minor adjustments were made to these assignments based on clustering behavior and functional similarity observed in the data.

Mutation profiling

Post-pET tumor samples were analyzed for somatic alterations using targeted next-generation sequencing, as previously described [12]. The analysis focused on a predefined panel of cancer-related genes. Variant calling was performed to identify recurrent genomic alterations (RGA), including mutations, amplifications, and deletions. Only alterations with a frequency of at least 7.5% in any treatment-response group were included for downstream analyses. Annotated variants were categorized by alteration type (e.g., missense, truncating) for integration with expression data. To evaluate the functional consequences of RGAs, baseline mRNA expression levels of affected genes were compared between wild-type and altered subgroups. Differences

in gene expression were assessed using the Wilcoxon rank sum test, and *p*-values were adjusted for multiple comparisons using FDR. Boxplots were used to visualize expression levels by RGA type (e.g., truncating vs. missense). In addition, to investigate the association between RGAs and NanoString BC360 signatures, signature scores were compared between wild-type and altered cases across the top 12 most frequently altered genes. The Wilcoxon rank sum test was applied to assess significance, and fdr-adjusted *p*-values were reported.

Factor Analysis of Mixed Data (FAMD)

FAMD is a dimensionality reduction technique used to analyze datasets containing both quantitative (numerical) and qualitative (categorical) variables (R package FactoMineR, version: 2.11) [15]. We used FAMD analyses to assess whether combined molecular and clinical features could distinguish endocrine response groups. Input variables included baseline NanoString BC360 signature scores, selected clinicopathological parameters, and recurrent genomic alterations (RGA). Analyses were conducted separately for the TAM and AI treatment cohorts.

Principal dimensions were computed to summarize variation across mixed data types (quantitative and qualitative). Sample distributions were visualized in two-dimensional space based on the top dimensions. Variable contributions to each dimension were quantified based on squared loadings for continuous variables and squared cosine values for categorical variables. The top contributing variables per dimension were used to interpret the main drivers of stratification.

Differential gene expression analysis

Differential expression analysis was performed using the NanoString BC360 panel, which includes 42 signature scores and 758 individual genes. Analyses were conducted separately for the TAM and AI treatment cohorts, as well as across distinct

Recurrence Score (RS) risk groups, to identify transcriptional differences associated with endocrine treatment response. Linear mixed models were used to compare responders (R) and non-responders (NR), adjusting for patient pair_id as a random effect (R package variancePartition, version: 1.24.1). Results were summarized as log2 fold changes with 95% confidence intervals (CI) and *p*-values. For the TAM cohort, *p*-values were further adjusted for multiple testing using FDR. Significant results were visualized as forest plots to highlight the direction and strength of association for each signature.

Survival analysis

Associations between NanoString BC360 gene expression signatures and survival endpoints as invasive disease-free survival (IDFS) and distant disease-free survival (DDFS) were analyzed within each treatment group using Cox proportional hazards models. Hazard ratios (HRs) with 95% confidence intervals (CI) and *p*-values were reported. Signatures were z-transformed prior to analysis. Results were visualized using the forestplot R package (version 3.1.3). No multiple testing correction was applied.

Statistical analysis

For the statistical analysis between the Responder and Non-Responder groups of the baseline clinicopathological characteristics, Cumulative Link Mixed Model (clmm from R package ordinal, version: 2023.12-4) with patient pair_id as a random effect was used to compare Ki67 at baseline, and Generalized Linear Mixed-Effects Models (glmer from R package lme4, version: 1.1-31) with patient pair_id as a random effect were used for all other comparisons. Linear Mixed-Effects Models (lmer from R package lme4, version: 1.1-31) with patient pair_id as a random effect were used to assess the discriminatory effect of FAMD dimensions on treatment response groups

or RS risk groups. The variance of log2-transformed signature scores across treatment and response groups was assessed and visualized. Wilcoxon rank-sum tests were used to compare signature scores between RGA groups.

The overall statistical strategy is explorative and hypothesis generating.

Results

Clinicopathological and Molecular Characteristics of the Cohort

We analyzed a cohort of 220 patients from the WSG-ADAPT trial, stratified by treatment with tamoxifen (TAM) or aromatase inhibitors (AI) and response status after three weeks of preoperative endocrine therapy. The cohort comprised 71 matched responder (R) and non-responder (NR) pairs and 78 unpaired samples (32 responders, 46 non-responders) (all the clinicopathological variables in Supplementary Table S2 Tab2). Clinicopathological features were overall well balanced between R and NR groups, with a few notable exceptions (statistical analyses of clinicopathological variables in Supplementary Table S1).

In the TAM cohort, non-responders were younger compared to responders ($p = 0.024$). Patients in the AI cohort were generally older than TAM cohort patients, and again, non-responders were significantly younger than responders ($p = 0.003$). PAM50 subtyping revealed a significant enrichment of the Luminal A subtype among TAM responders, while Luminal B was more frequent in TAM non-responders ($p = 0.044$). Tumor-infiltrating lymphocytes (TILs) were significantly lower in TAM non-responders compared to responders ($p = 0.023$).

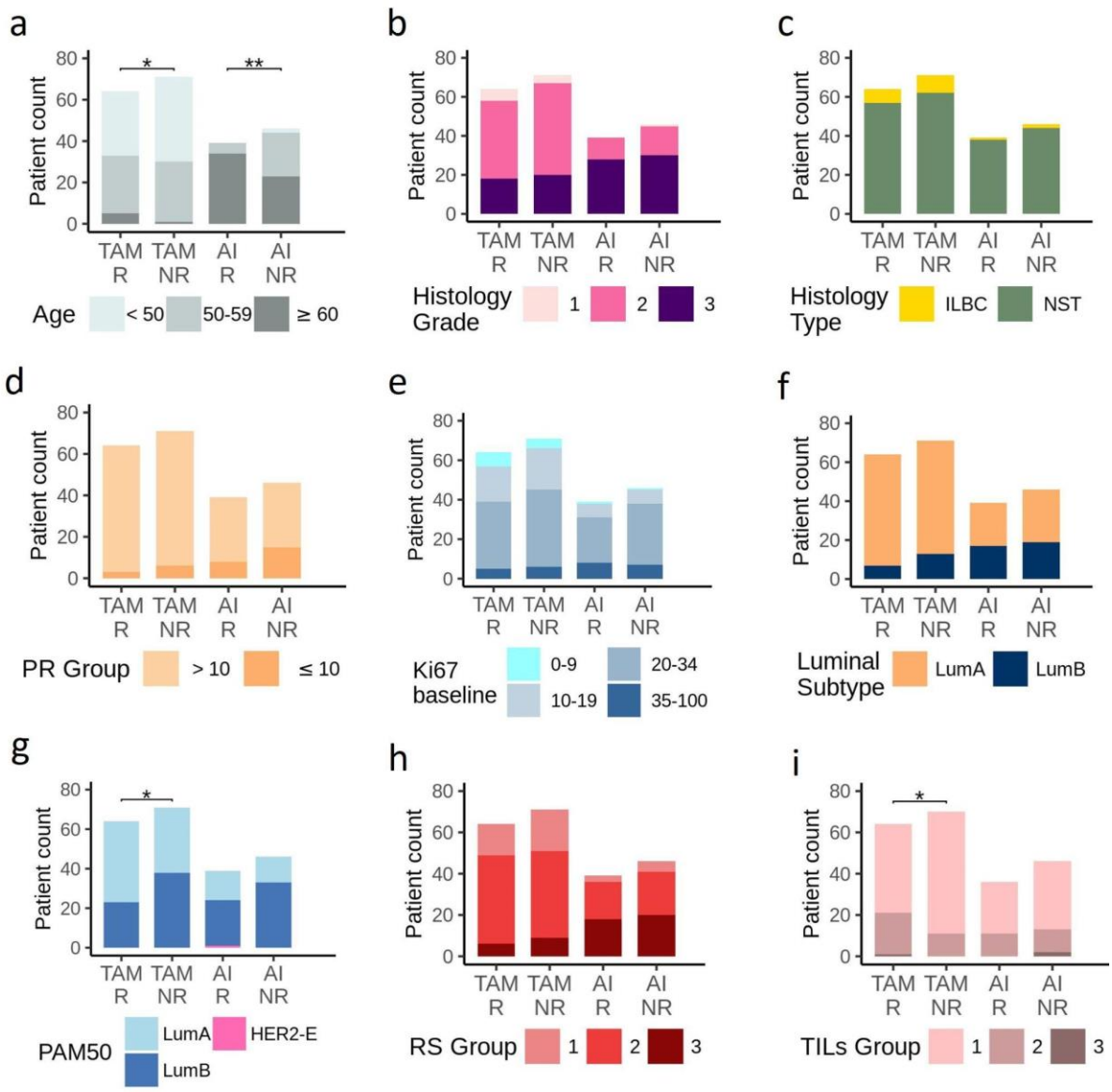

Fig. 1: Descriptive statistics of the cohort.

Distribution of patients (n=220), analyzed at baseline prior to treatment with TAM (n = 135) or AI (n = 85). Patients are stratified by later response to short-term pET into responder (R) and non-responder (NR) according to: (a) age; (b) histology grade; (c) histology type; (d) progesterone receptor (PR) status; (e) percentage of Ki67-positive staining in IHC at baseline; (f) luminal subtype; (g) intrinsic subtypes of breast cancer using PAM50 gene expression signatures; (h) recurrence score (RS); (i) tumor-infiltrating lymphocytes in pathologic tissue sections (TILs, patients without data are excluded). Statistical analysis using Generalized Linear Mixed-Effects Models (glmer) with patient pair_id as a random effect (Cumulative Link

Mixed Model (clmm) with patient pair_id as a random effect for (e)). Asterisks *, **, *** indicate *p*-values < 0.05, 0.01, 0.001.

Baseline NanoString BC360 gene expression signatures (Supplementary Table S2 Tab4) were assessed by visualizing the distribution of 42 signature scores across treatment response groups (Supplementary Fig. S1). Progesterone receptor (PGR) expression scores were reduced, and BC proliferation scores were elevated in the AI groups compared to the TAM groups, consistent with immunohistochemical findings of reduced PR and elevated baseline Ki67 expression. Overall, we noted that the AI cohort exhibited greater variability in signature scores compared to the TAM cohort, especially for the PGR signature score, indicating higher heterogeneity in the cohort (Supplementary Fig. S2).

Taken together, our findings indicated that patient age, PAM50 luminal subtype, immune infiltration, and transcriptional variability are associated with endocrine treatment response. Despite the observed differences, overall distribution of clinicopathological features remained balanced, validating the comparability of response groups within treatment arms.

Key clinical and molecular features correlated with baseline NanoString signatures

To characterize the molecular landscape in the TAM and AI cohorts, we performed Spearman's correlations between baseline NanoString BC360 gene expression signatures, clinicopathological features, and PAM50 subtypes (Fig. 2, Supplementary Table S2 Tab5-6).

a
TAM
Block
A
B
C
1
0.8
0.6
0.4
0.2
0
-0.2
-0.4
-0.6
-0.8
-1

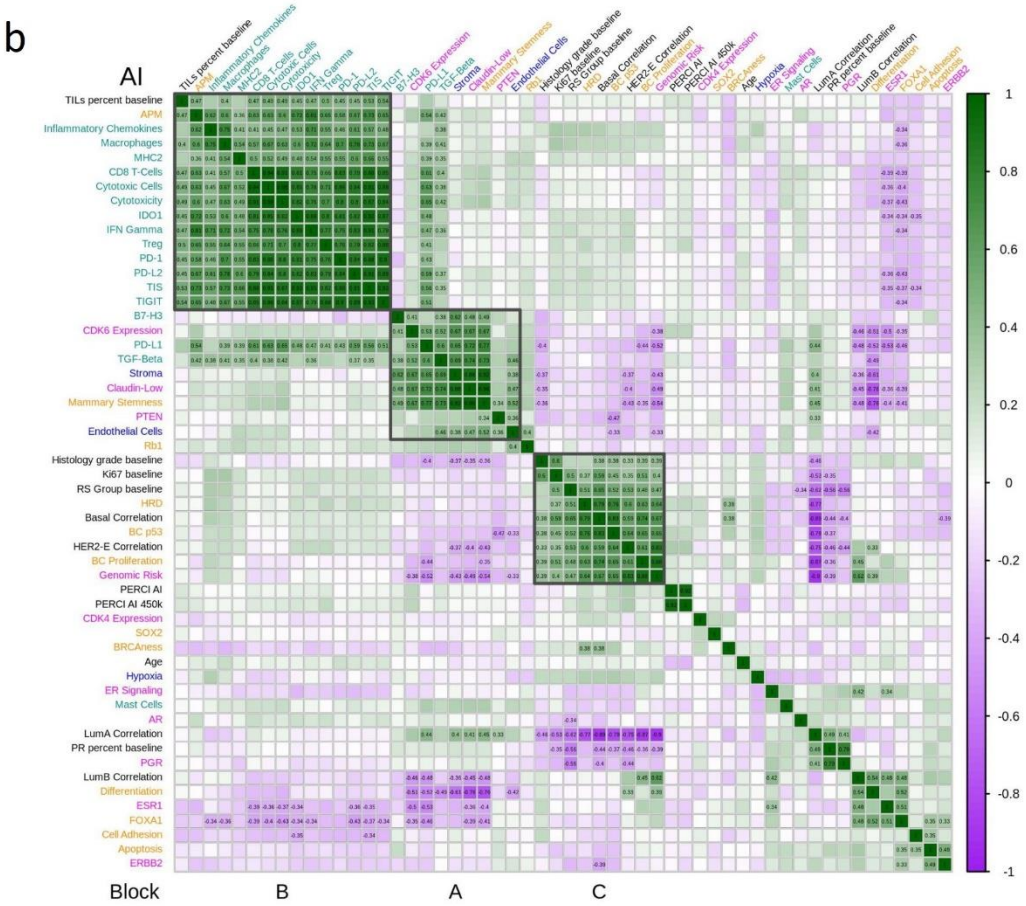
b
AI
Block
B
A
C
1
0.8
0.6
0.4
0.2
0
-0.2
-0.4
-0.6
-0.8
-1

Fig. 2: Associations of gene expression signatures with clinico-pathological parameters and PAM50 correlations.

Spearman's correlation coefficients were calculated between NanoString gene expression signatures (color coded by four NanoString categories: tumor (orange), immune (dark cyan), microenvironment (blue) and breast cancer (magenta)), selected clinical features, PERCI, RS score, and correlation values to the PAM50 subtypes (all black) in the TAM cohort (a) and AI cohort (b). Correlations are indicated by a color gradient from purple (-1) to green (1). Results with statistically significant differences between response groups are highlighted by numerical correlation coefficients (two-tailed test of significance which compares the observed value of correlation coefficient to its expected value under the null hypothesis (no correlation between the two variables), fdr-adjusted *p*-value < 0.01). Further details are described in the Methods section.

Based on unsupervised clustering of the correlation matrix, the NanoString gene expression signatures were segregated into three major functional blocks (Supplementary Table S2 Tab3): Block A (reactive tumor microenvironment), Block B (immune response), and Block C (proliferation and genomic risk). Additional signatures, which did not form strong clusters, were grouped into Block D (tumor-related signatures, colored in orange in Fig. 2) and Block E (hormone and breast cancer-related signatures, colored in magenta in Fig. 2), following NanoString's predefined biological categories.

Block A demonstrated consistent signature expression related to stromal and microenvironmental activity, including signatures B7-H3, CDK6 Expression, Claudin-Low, Endothelial Cells, Mammary Stemness, Mast Cells, PD-L1, PTEN, Stroma, and TGF-Beta. Block B consisted of immune-related signatures such as APM (Antigen processing machinery), CD8 T-Cells, Cytotoxic Cells, Cytotoxicity, IDO1, IFN Gamma,

Inflammatory Chemokines, Macrophages, MHC-II, PD-1, PD-L2, TIGIT, TIS (Tumor Inflammation Signature), and Treg, as well as the clinical feature TILs percent at baseline. Block C contained signatures and features associated with proliferation and genomic instability, including signatures BC p53, BC Proliferation, Genomic Risk, HRD (Homologous recombination deficiency), as well as clinical and molecular markers such as RS group, histologic grade, Ki67 at baseline, and PAM50 subtype correlations of Luminal B, HER2-enriched, and Basal-like. The Predictive Endocrine Resistance Index (PERCI) [12] also strongly correlated with Block C components.

Multiple consistent and statistically significant correlations were observed between NanoString BC360 gene expression signatures and clinical parameters. Notably, TILs percent showed strong correlations with immune response signatures from block A (e.g., TIS, IFN Gamma, Macrophages) (TAM: $\rho = 0.27$ to 0.38; AI: $\rho = 0.4$ to 0.54) in both treatment groups, indicating concordance between histopathological measures of immune infiltration and molecular signatures of immune activation.

The Differentiation signature was strongly negatively correlated with block A signatures (TAM: $\rho = -0.30$ to -0.71; AI: $\rho = -0.49$ to -0.76), whereas Luminal A correlation was highly negatively correlated with proliferation and genomic risk signatures in block C (TAM: $\rho = -0.38$ to -0.93; AI: $\rho = -0.46$ to -0.90). PR percent positive staining at baseline was strongly correlated with PGR signature expression (TAM: $\rho = 0.6$; AI: $\rho = 0.79$), indicating good concordance between immunohistochemistry and transcriptomic data.

These findings demonstrate that baseline gene expression signatures robustly reflect established clinicopathological features and molecular subtypes in ER+ breast cancer and support their utility for stratifying tumors by biological behavior.

Recurrent genomic alterations and their functional impact on gene expression

Recurrent genomic alterations (RGA) were analyzed in post-pET tumor samples (Supplementary Table S2 Tab7), stratified by treatment group and response status, to uncover genomic features linked to endocrine therapy resistance. The analysis focused on alterations with a recurrence of at least 7.5% in any subgroup. These alterations spanned multiple alteration types, including amplifications, deletions, and missense, truncating or splicing mutations (Fig. 3a). Several genes showed significantly higher alteration frequencies in non-responders compared to responders, including *BRCA2* and *CCND1* in the TAM group, and *ESR1*, *FGFR2*, *RB1* and *TP53* in the AI group. Interestingly, *CBFB* and *RYR2* were more frequently mutated in TAM responders (Fig. 3b). To evaluate the functional relevance of these alterations, we analyzed baseline mRNA expression levels of the corresponding NanoString BC360 genes (Supplementary Table S2 Tab8). In the TAM cohort, non-responder tumors with truncating mutation or deletion of *BRCA2* exhibited significantly lower *BRCA2* mRNA expression, while *CCND1* amplification was associated with significantly elevated *CCND1* transcript levels.

In the AI cohort, mRNA expression of *ESR1* and *FGFR2* was significantly increased in cases with amplifications of these genes. Truncating mutations of the *RB1* gene were linked with reduced *RB1* expression. Similarly, *TP53* gene truncations, observed in both treatment cohorts, were consistently associated with decreased *TP53* mRNA levels, indicating potential loss of function of this tumor suppressor gene (Fig. 3c-h). In addition, *CDH1* truncating mutations in the TAM cohort were significantly associated with reduced *CDH1* expression in both response groups (Supplementary Fig. S3), further supporting the functional consequence of specific alterations on mRNA expression.

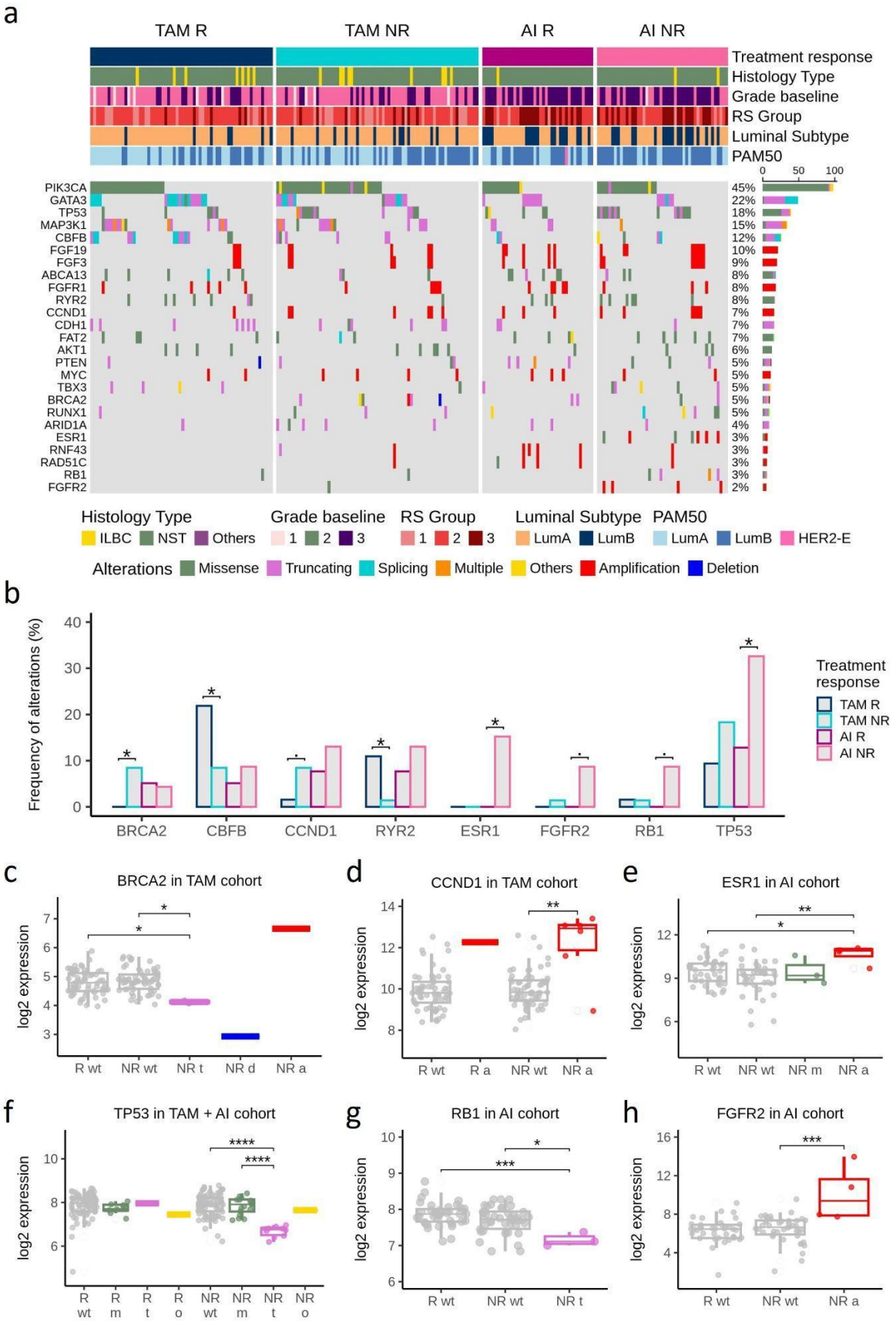
a
TAM R
TAM NR
AI R
AI NR
Treatment response
Histology Type
Grade baseline
RS Group
Luminal Subtype
PAM50
PIK3CA 45%
GATA3 22%
TP53 18%
MAP3K1 15%
CBFB 12%
FGF19 10%
FGF3 9%
ABCA13 8%
FGFR1 8%
RYR2 8%
CCND1 7%
CDH1 7%
FAT2 7%
AKT1 6%
PTEN 5%
MYC 5%
TBX3 5%
BRCA2 5%
RUNX1 5%
ARID1A 4%
ESR1 3%
RNF43 3%
RAD51C 3%
RB1 3%
FGFR2 2%
Histology Type: ILBC NST Others
Grade baseline: 1 2 3
RS Group: 1 2 3
Luminal Subtype: LumA LumB
PAM50: LumA LumB HER2-E
Alterations: Missense Truncating Splicing Multiple Others Amplification Deletion
b
Frequency of alterations (%)
BRCA2 CBFB CCND1 RYR2 ESR1 FGFR2 RB1 TP53
Treatment response
TAM R
TAM NR
AI R
AI NR
c
BRCA2 in TAM cohort
log2 expression
R wt NR wt NR t NR d NR a
d
CCND1 in TAM cohort
R wt R a NR wt NR a
e
ESR1 in AI cohort
R wt NR wt NR m NR a
f
TP53 in TAM + AI cohort
R wt R m R t R o NR wt NR m NR t NR o
g
RB1 in AI cohort
R wt NR wt NR t
h
FGFR2 in AI cohort
R wt NR wt NR a

Fig. 3: Recurrent genomic alterations (RGA) and expression of significantly altered genes.

(a) The oncoprint summarizes the mutational landscape of recurrent genomic alterations in the present study, color-coded by the RGA type and separated into TAM R, TAM NR, AI R and AI NR groups. Tumor specimens derived after short-term pET were analyzed for genomic alterations. Genes are sorted by total alteration burden (mutations, amplifications and deletions). Only RGA at minimum 7.5% recurrence in either subgroup are shown. The barplot at the right quantifies the recurrence of the RGA. Clinical annotations of cases are indicated on the top. (b) Frequencies of RGA with significant differences between NR and R groups, analyzed using Fisher-exact test with *, *p*-value < 0.05. (c - h) NanoString log2 mRNA expression levels at baseline before pET of RGA with significant differences between NR and R groups, separated by RGA types and analyzed using Wilcoxon rank sum test with •, *, **, ***, ****, *p*-values < 0.1, 0.05, 0.01, 0.001, 0.0001. Expression data for CBFB and RYR2 are not available. Boxplots display the median (line), interquartile range (box), and whiskers extending to 1.5 times the interquartile range (IQR). RGA types: amplification (a), deletion (d), missense (m), truncating (t), others (o).

Together, these results identify recurrent genomic alterations that are significantly enriched in responders or non-responders, respectively, and have measurable effects on gene expression at baseline, underscoring their potential role in mediating endocrine resistance.

Associations between recurrent genomic alterations and NanoString signatures

Associations between RGAs and baseline NanoString BC360 signatures were tested by comparing signature scores between wild-type and altered samples for the 12 most frequently mutated genes (Fig. 4, Supplementary Table S2 Tab9). Alterations in *TP53* were linked with increased expression of immune-associated signatures (Block B) in both treatment groups and proliferation-associated signatures (Block C) in the TAM

cohort. When stratifying *TP53* alterations into truncating and missense mutations, distinct expression patterns emerged, with missense mutations showing a stronger association with increased signature expression in functional blocks B and C. These findings were consistent with reduced *TP53* mRNA levels reported in altered samples (Fig. 3f). In contrast, mutations in some of the most recurrently mutated genes, *PIK3CA1*, *GATA3* and *MAP3K1,* were associated with lower expression of immune- (Block B) and proliferation-related signatures (Block C), whereas *CCND1* amplifications led to increased expression of these signatures.

In the AI cohort, fewer statistically significant associations were detected, possibly due to higher variance in the signature scores (Supplementary Fig. S2). *PIK3CA1* alterations were associated with higher expression of tumor microenvironment-related signature scores (Block A). *MAP3K1* alterations were linked with enhanced cell adhesion signature in Block D, and consistent with the TAM group, with lower expression of immune-related signatures scores (Block B).

These results suggest that the presence of recurrent genomic alterations, particularly involving *TP53* and *CCND1*, contributes to the observed differences in baseline NanoString gene expression signatures, offering mechanistic insights into the molecular heterogeneity associated with primary endocrine resistance.

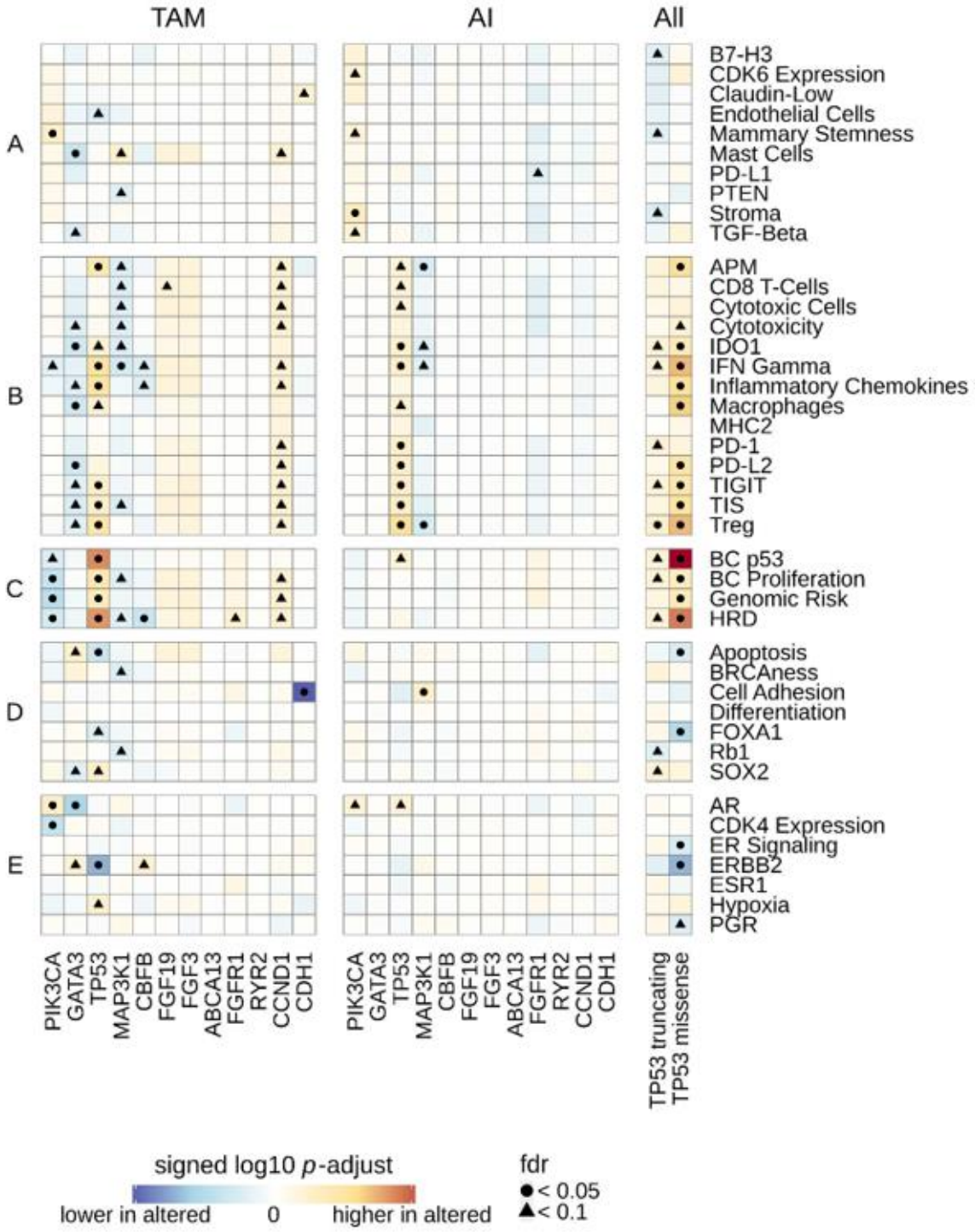

Fig. 4: Comparison of NanoString signatures between wild type and RGA groups.

Influence of the top 12 altered genes (from Fig. 3) on NanoString signature scores. Wilcoxon test for comparison of NanoString signature scores between wild type samples and samples

with alterations. For “All”, samples of the TAM and AI cohorts were combined. Fdr-adjusted *p*-value as indicated. Blocks A to E are as described in legend of Fig. 2.

Integration of molecular, clinical, and genomic features *via* FAMD reveals key contributors to patient stratification

Factor analysis of mixed data (FAMD) is a factorial method that allows joint analysis of quantitative and qualitative variables [15]. FAMD was performed separately for the TAM and AI cohorts to evaluate the joint contribution of NanoString signatures, clinicopathological variables, and RGAs to patient heterogeneity (Fig. 5, Fig. 6). This multivariate approach allowed us to explore whether combined molecular and clinical profiles could distinguish treatment response groups.

In the TAM cohort, FAMD revealed partial separation of responders and non-responders along the first three principal dimensions: Dim1 (18.7%), Dim2 (13.9%), and Dim3 (7.8%) (values of Dim1 to Dim3 in Supplementary Table S2 Tab10) (Fig. 5a, 5d). Among the quantitative features, immune-related signatures including TIS, PD-L2, and TIGIT (Block B), as well as Genomic Risk and BC Proliferation (Block C), showed strong contributions to the primary dimensions. Additional contributors included Stroma and Mammary Stemness (Block A), and Luminal A correlation (Fig. 5b, 5e). Qualitative variables with the greatest influence included mutations in *TP53*, *CCND1*, *GATA3*, *PIK3CA*, and *RYR2*, and amplifications in *FGF3*, *FGF19*, and *FGFR1*, along with *PIK3CA* wild-type status (Fig. 5c, 5f).

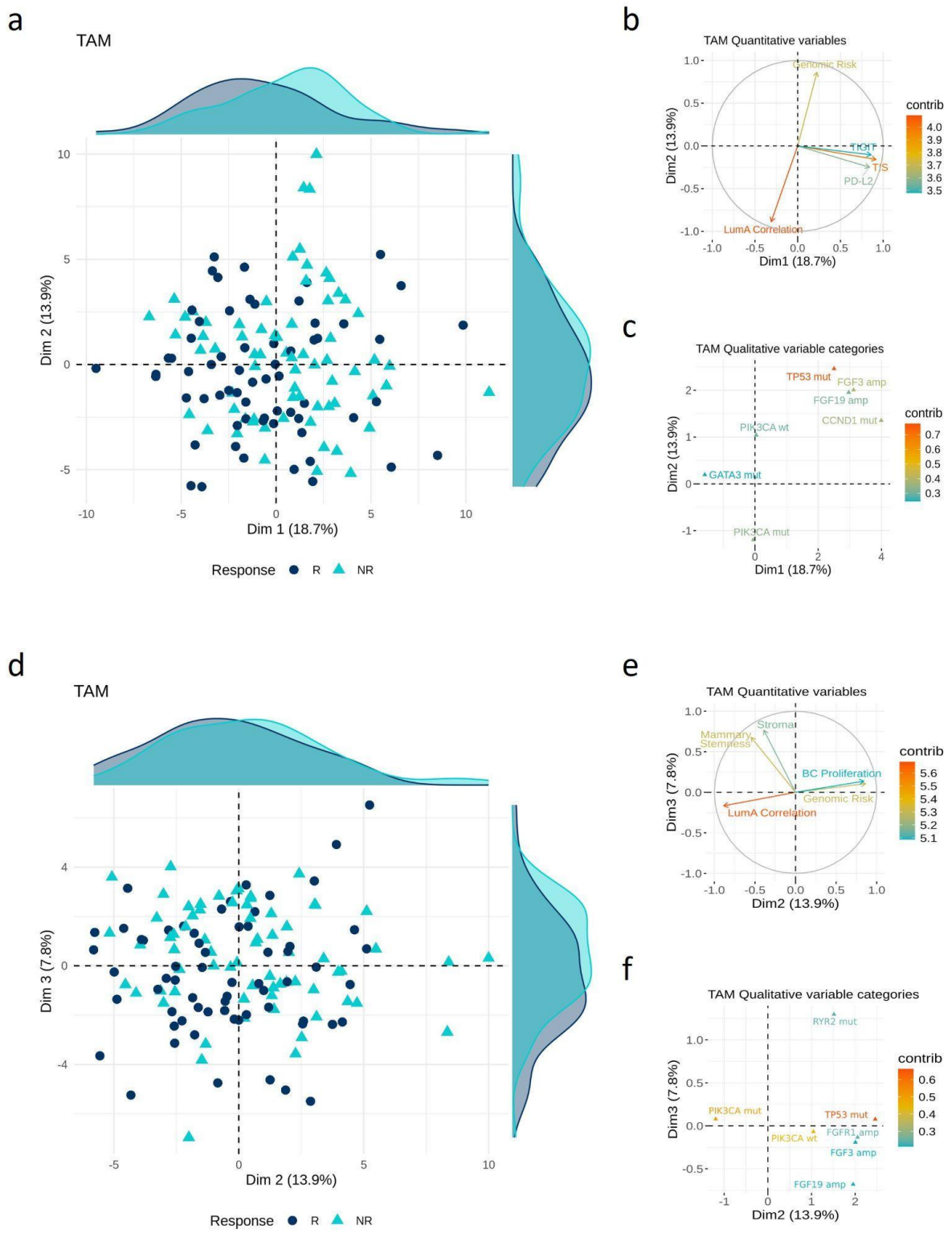

Fig. 5: Factor analysis of mixed data (FAMD) in the TAM cohort.

(a and d) Distribution of samples in Dim1 vs. Dim2 (a) and in Dim2 vs. Dim3 (d) based on their NanoString signature scores, RGAs and clinico-pathological characteristics in a two-dimensional space using FAMD. Responders (R) and non-responders (NR) are indicated by

different colors and shapes. Density curves at the outside of the plots indicate patient counts. (b and e) Biplot of quantitative variables. Arrows indicate the five most important signatures. (c and f) Biplot of seven top qualitative variable categories. The strength of the contribution is indicated by the color gradient. Dimensions are labeled on the axes, and the percentage of the contributions is given in parentheses.

In the AI cohort, a similar trend of partial separation by response groups was observed, although with slightly less pronounced discrimination than in the TAM cohort (Dim1: 21.2%, Dim2: 14.1%, Dim3: 6.5%, values of Dim1 to Dim3 in Supplementary Table S2 Tab11) (Fig. 6a, 6d). Key quantitative variables contributing to stratification included immune-related signatures (TIS, PD-L2, Cytotoxic Cells; Block B), PD-L1 (Block A), and signatures Genomic Risk and BC p53 (Block C). Basal-like and Luminal A correlations also featured among the top contributors (Fig. 6b, 6e). Among qualitative features, mutations in *TP53*, *CCND1*, *PIK3CA*, *CBFB*, *CDH1*, *MAP3K1*, and *RYR2*, as well as *FGFR1* amplification and ILBC histology, emerged as major contributors (Fig. 6c, 6f).

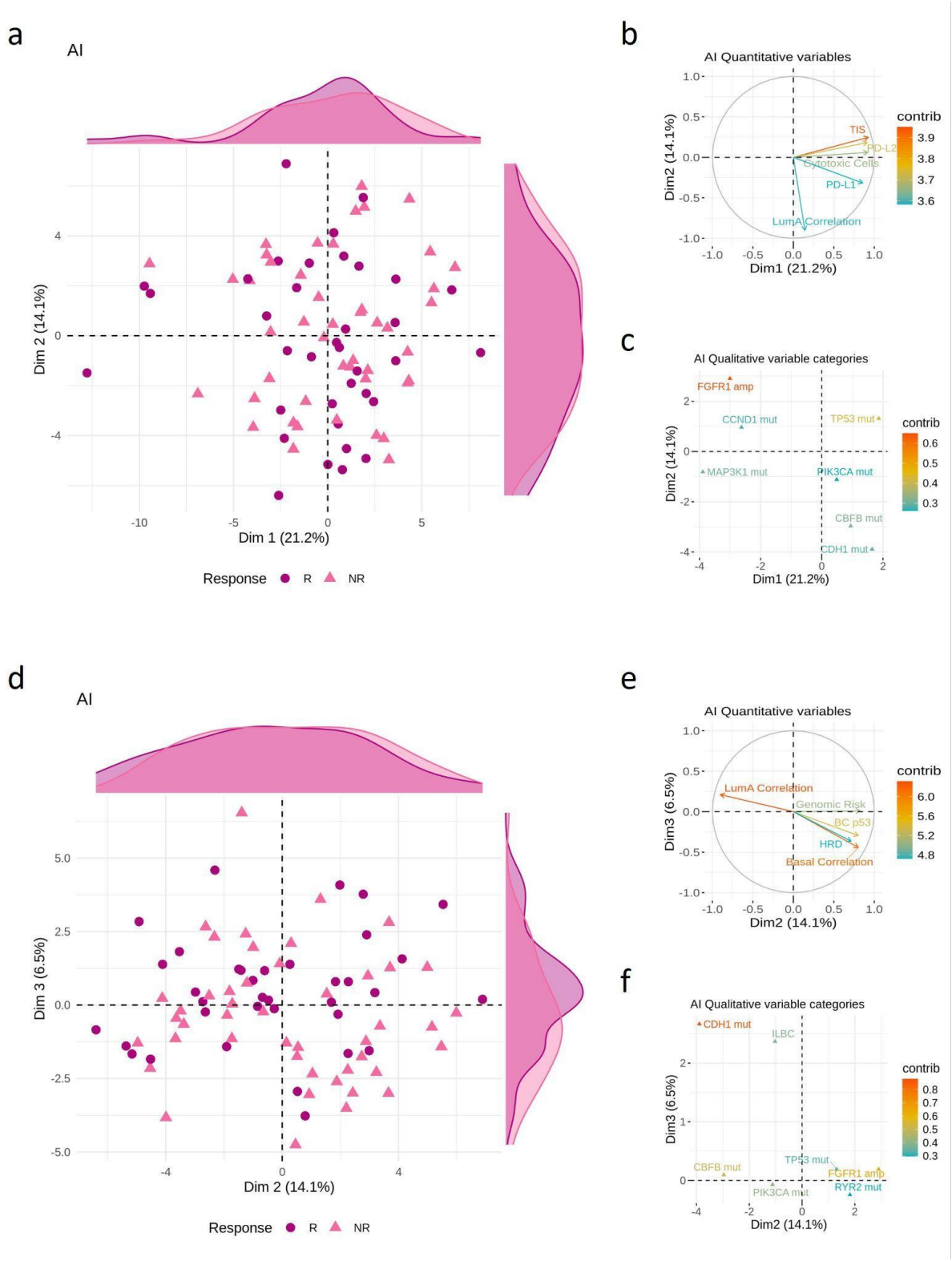

Fig. 6: Factor analysis of mixed data (FAMD) in the AI cohort.

(a and d) Distribution of samples in Dim1 vs. Dim2 (a) and in Dim2 vs. Dim3 (d) based on their signature expression scores, RGAs and clinico-pathological characteristics in a two-dimensional space using FAMD. Responders (R) and non-responders (NR) are indicated by

different colors and shapes. Density curves at the outside of the plots indicate patient counts. (b and e) Biplot of quantitative variables. Arrows indicate the five most important signatures. (c and f) Biplot of seven top qualitative variable categories. The strength of the contribution is indicated by the color gradient. Dimensions are labeled on the axes, and the percentage of the contributions is given in parentheses.

The relative influence of each feature was quantified by assessing their contributions to the first two dimensions of the FAMD across both cohorts (Supplementary Fig. S4, Supplementary Table S2 Tab12-13). Proliferation and immune-related signatures were consistently among the strongest drivers of variance.

In addition to treatment response, we stratified patients into four risk groups based on Recurrence Score (RS) and age: RS1 (low risk with RS score = 1), RS2.1 (intermediate risk with RS score = 2 and age less than or equal to 51 years), RS2.2 (intermediate risk with RS score = 2 and age above 51 years) and RS3 (high risk with RS score = 3) (distribution of treatment response, PAM50 subtypes and age in the four groups in Supplementary Fig. S5a-c). We conducted an additional FAMD using this RS risk group information as a stratification variable (Supplementary Fig. S5d-g). As indicated by density curves at the outside of the plots and linear mixed models, RS risk grouping resulted in better sample separation than classification by treatment response, especially for dimensions 1 and 2 in the TAM group and dimensions 2 and 3 in the AI group (lmer results in Supplementary Table S2 Tab14-17).

Taken together, these analyses illustrate the value of integrating molecular, clinical, and genomic features to uncover cohort substructures. They further suggest that immune and proliferation signatures, along with specific driver alterations may more accurately reflect the underlying tumor biology than endocrine response status alone.

Differential expression of NanoString signatures stratified by treatment response

Differential expression analysis of NanoString gene expression signatures between responder and non-responder groups was conducted in the TAM and AI cohorts to validate molecular features linked to endocrine therapy response (Supplementary Table S2 Tab18-19). This analysis built on previous findings from the FAMD and correlation analyses to determine which baseline transcriptional features distinguished response groups.

In the TAM cohort, several signatures were significantly (fdr < 0.01) upregulated in non-responders (Fig. 7a). These included immune-related signatures from Block B, such as APM (log2FC [95% CI] = 0.54 [0.24-0.84]), IFN Gamma (log2FC = 0.54 [0.24-0.84]), Treg (log2FC = 0.46 [0.18-0.73]) and Inflammatory Chemokines (log2FC = 0.36 [0.11-0.62]), as well as signatures Genomic Risk (log2FC = 0.43 [0.18-0.68]), BC Proliferation (log2FC = 0.38 [0.17-0.58]), and B7-H3 (log2FC = 0.19 [0.06-0.32]) from Block C. The BC p53 tumor signature also showed significant differential expression (log2FC = 0.23 [0.06-0.39]), consistent with our previous findings linking *TP53* alterations and expression to treatment resistance [16,17].

In the AI cohort, due to wider confidence intervals, fewer signatures demonstrated significant (*p*-value < 0.05) differences between responders and non-responders (Fig. 7b). Associations were observed for the Block C signatures BC p53 (log2FC = 0.24 [0.03-0.46]), Genomic Risk (log2FC = 0.23 [0.04-0.43]), BC Proliferation, HRD, and CDK6 expression (Block A), echoing the contribution of proliferation-related signatures identified in the AI cohort FAMD analysis. Additionally, Rb1 signature (Block D) was associated with better treatment response (log2FC = -0.21 [-0.38 - -0.04]).

For comparison, we further performed a differential signature score analysis stratifying the patients by RS risk groups (Supplementary Fig. S6, Supplementary Table S2 Tab20-23). In the low risk group RS1, proliferation- and immune-related signatures, as well as ER Signaling (log2FC = 0.37 [0.07-0.67]) were significantly (*p*-value < 0.05) upregulated in non-responders. In the intermediate risk group RS2.1 of younger women (age ≤ 51), a broad set of signatures, spanning immune, proliferative, and stromal processes, were significantly elevated in the non-responder group, as well as Mast cells (log2FC = 0.86 [0.34-1.38]) and Mammary Stemness signatures (log2FC = 0.55 [0.1-1.01]). In contrast, the older age (age > 51 years) intermediate-risk group RS2.2 and the high-risk group RS3 exhibited few significant differences between the response groups, suggesting limited signature-based discrimination in these RS-stratified groups. High SOX2 (log2FC = 0.79 [0.2-1.38]) and CDK6 expression (log2FC = 0.48 [0.17-0.8]) indicated worse response in risk group RS2.2, whereas high PD-1 expression was suggestive of better response (log2FC = -0.58 [-1.06 - -0.09]) in RS3 group cases.

a

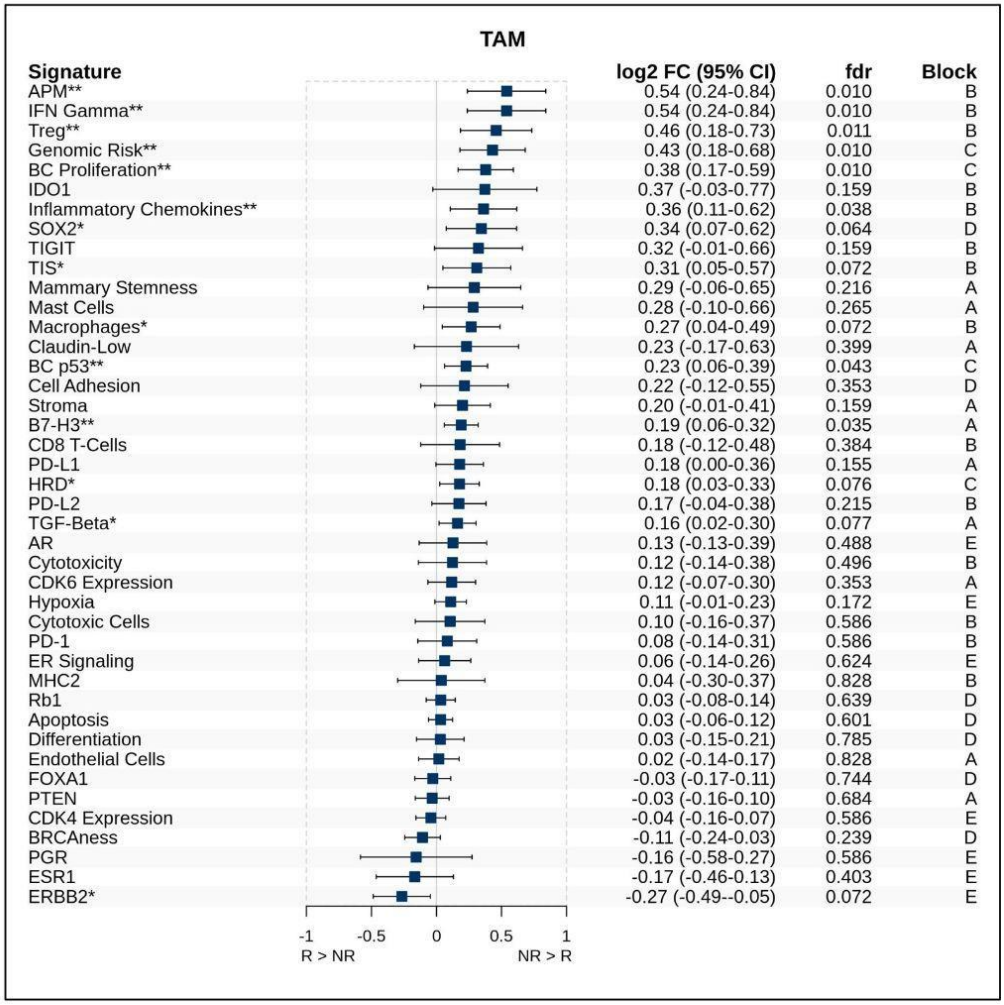

Signature	log2 FC (95% CI)	fdr	Block
APM**	0.54 (0.24-0.84)	0.010	B
IFN Gamma**	0.54 (0.24-0.84)	0.010	B
Treg**	0.46 (0.18-0.73)	0.011	B
Genomic Risk**	0.43 (0.18-0.68)	0.010	C
BC Proliferation**	0.38 (0.17-0.59)	0.010	C
IDO1	0.37 (-0.03-0.77)	0.159	B
Inflammatory Chemokines**	0.36 (0.11-0.62)	0.038	B
SOX2*	0.34 (0.07-0.62)	0.064	D
TIGIT	0.32 (-0.01-0.66)	0.159	B
TIS*	0.31 (0.05-0.57)	0.072	B
Mammary Stemness	0.29 (-0.06-0.65)	0.216	A
Mast Cells	0.28 (-0.10-0.66)	0.265	A
Macrophages*	0.27 (0.04-0.49)	0.072	B
Claudin-Low	0.23 (-0.17-0.63)	0.399	A
BC p53**	0.23 (0.06-0.39)	0.043	C
Cell Adhesion	0.22 (-0.12-0.55)	0.353	D
Stroma	0.20 (-0.01-0.41)	0.159	A
B7-H3**	0.19 (0.06-0.32)	0.035	A
CD8 T-Cells	0.18 (-0.12-0.48)	0.384	B
PD-L1	0.18 (0.00-0.36)	0.155	A
HRD*	0.18 (0.03-0.33)	0.076	C
PD-L2	0.17 (-0.04-0.38)	0.215	B
TGF-Beta*	0.16 (0.02-0.30)	0.077	A
AR	0.13 (-0.13-0.39)	0.488	E
Cytotoxicity	0.12 (-0.14-0.38)	0.496	B
CDK6 Expression	0.12 (-0.07-0.30)	0.353	A
Hypoxia	0.11 (-0.01-0.23)	0.172	E
Cytotoxic Cells	0.10 (-0.16-0.37)	0.586	B
PD-1	0.08 (-0.14-0.31)	0.586	B
ER Signaling	0.06 (-0.14-0.26)	0.624	E
MHC2	0.04 (-0.30-0.37)	0.828	B
Rb1	0.03 (-0.08-0.14)	0.639	D
Apoptosis	0.03 (-0.06-0.12)	0.601	D
Differentiation	0.03 (-0.15-0.21)	0.785	D
Endothelial Cells	0.02 (-0.14-0.17)	0.828	A
FOXA1	-0.03 (-0.17-0.11)	0.744	D
PTEN	-0.03 (-0.16-0.10)	0.684	A
CDK4 Expression	-0.04 (-0.16-0.07)	0.586	E
BRCAness	-0.11 (-0.24-0.03)	0.239	D
PGR	-0.16 (-0.58-0.27)	0.586	E
ESR1	-0.17 (-0.46-0.13)	0.403	E
ERBB2*	-0.27 (-0.49--0.05)	0.072	E

b

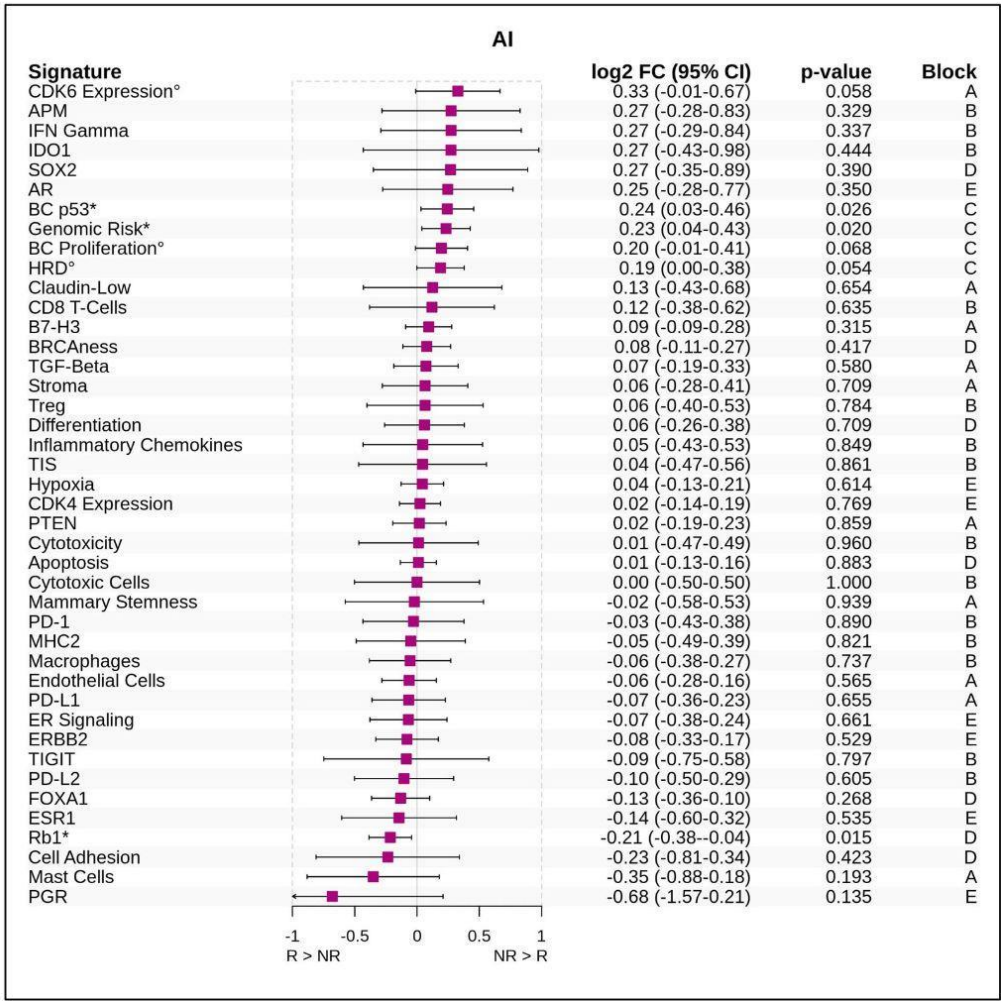

Signature	log2 FC (95% CI)	p-value	Block
CDK6 Expression°	0.33 (-0.01-0.67)	0.058	A
APM	0.27 (-0.28-0.83)	0.329	B
IFN Gamma	0.27 (-0.29-0.84)	0.337	B
IDO1	0.27 (-0.43-0.98)	0.444	B
SOX2	0.27 (-0.35-0.89)	0.390	D
AR	0.25 (-0.28-0.77)	0.350	E
BC p53*	0.24 (0.03-0.46)	0.026	C
Genomic Risk*	0.23 (0.04-0.43)	0.020	C
BC Proliferation°	0.20 (-0.01-0.41)	0.068	C
HRD°	0.19 (0.00-0.38)	0.054	C
Claudin-Low	0.13 (-0.43-0.68)	0.654	A
CD8 T-Cells	0.12 (-0.38-0.62)	0.635	B
B7-H3	0.09 (-0.09-0.28)	0.315	A
BRCAness	0.08 (-0.11-0.27)	0.417	D
TGF-Beta	0.07 (-0.19-0.33)	0.580	A
Stroma	0.06 (-0.28-0.41)	0.709	A
Treg	0.06 (-0.40-0.53)	0.784	B
Differentiation	0.06 (-0.26-0.38)	0.709	D
Inflammatory Chemokines	0.05 (-0.43-0.53)	0.849	B
TIS	0.04 (-0.47-0.56)	0.861	B
Hypoxia	0.04 (-0.13-0.21)	0.614	E
CDK4 Expression	0.02 (-0.14-0.19)	0.769	E
PTEN	0.02 (-0.19-0.23)	0.859	A
Cytotoxicity	0.01 (-0.47-0.49)	0.960	B
Apoptosis	0.01 (-0.13-0.16)	0.883	D
Cytotoxic Cells	0.00 (-0.50-0.50)	1.000	B
Mammary Stemness	-0.02 (-0.58-0.53)	0.939	A
PD-1	-0.03 (-0.43-0.38)	0.890	B
MHC2	-0.05 (-0.49-0.39)	0.821	B
Macrophages	-0.06 (-0.38-0.27)	0.737	B
Endothelial Cells	-0.06 (-0.28-0.16)	0.565	A
PD-L1	-0.07 (-0.36-0.23)	0.655	A
ER Signaling	-0.07 (-0.38-0.24)	0.661	E
ERBB2	-0.08 (-0.33-0.17)	0.529	E
TIGIT	-0.09 (-0.75-0.58)	0.797	B
PD-L2	-0.10 (-0.50-0.29)	0.605	B
FOXA1	-0.13 (-0.36-0.10)	0.268	D
ESR1	-0.14 (-0.60-0.32)	0.535	E
Rb1*	-0.21 (-0.38--0.04)	0.015	D
Cell Adhesion	-0.23 (-0.81-0.34)	0.423	D
Mast Cells	-0.35 (-0.88-0.18)	0.193	A
PGR	-0.68 (-1.57-0.21)	0.135	E

Fig 7. Differential expression of NanoString gene signatures between response groups.

Summary of differential NanoString gene signatures expression between response groups in the TAM (a) and AI (b) cohort by fitting linear mixed models with patient pair_id as a random effect. The following variables are used as covariates: TAM: age group and TILs group at baseline; AI: age group. Signatures are sorted by log2 fold change of mean signature expression between responders and non-responders per treatment. Significant signatures are indicated by °, *, ** with *p*-values < 0.1, 0.05, 0.01 (fdr < 0.05 for TAM). 95% confidence intervals, (fdr-adjusted) *p*-values and block membership are shown.

To complement the signature-level findings, gene-level differential expression analysis was performed (Supplementary Fig. S7, Supplementary Table S2 Tab24-25). In the TAM cohort, several genes implicated in immune signaling and tumor–immune interaction, such as *COL11A1*, *ISG15, OAS3, CCL8*, and *CXCL10*, were significantly upregulated in non-responders. Additionally, genes associated with cellular response to hypoxia, including *ARNT2* and *SIX1*, also showed higher expression in non-responders (all with log2FC > 0.590, fdr < 0.05). In the AI cohort, fewer genes reached statistical significance. However, several genes were notably upregulated in non-responders (all with log2FC > 0.538, *p*-value < 0.05), including *B3GNT3* linked to immune cell trafficking, *NFKBIZ* involved in inflammation and apoptosis, and the proliferation- and hypoxia-associated genes *TMPRSS4* and *SMC1B*.

Together, these results demonstrate that distinct transcriptional programs, particularly those related to immune activation and proliferation, differ between treatment response groups and that their relevance may vary by RS risk groups and treatment context. These findings support the utility of both gene signatures and individual gene markers for understanding endocrine response heterogeneity.

Baseline NanoString gene expression signatures are associated with long-term survival outcomes

The median follow-up duration for our cohort was 59.8 months, with follow-up data available for 191 patients from the total 220 patients included in the study. The prognostic significance of baseline transcriptional profiles was examined by linking NanoString signature scores to invasive (IDFS) and distant disease-free survival (DDFS), in both the TAM and AI cohorts (Fig. 8). In the TAM cohort, the number of events is still very low (n=4) and longer follow-up times might reveal additional associations [18]. Higher TGF-Beta (HR [with 95% CI] = 5.09 [1.29-20.14]) and CDK6 (HR = 3.68 [1.22-11.09]) signature scores correlated with worse IDFS and DDFS, suggesting their roles in facilitating disease recurrence. In contrast, higher baseline expression of the PGR signature was associated with improved survival, in line with its established prognostic role in ER-positive breast cancer (Fig. 8a).

In the AI cohort, the BC p53 signature score (HR = 2.74 [1.08-6.94]) was the strongest prognosticator for IDFS, whereas *TP53* mutations alone were not prognostically significant (data not shown). In addition, Genomic Risk (HR = 2.5 [1.07-5.83]), HRD (HR = 2.44 [1.12-5.29]), and Hypoxia (HR = 1.99 [1.12-3.51]) signature scores were associated with worse IDFS (Fig. 8b). For DDFS, poor survival outcomes were linked to higher ERBB2 (HR = 2.46 [1.05-5.75]) and Hypoxia (HR = 2.12 [1.17-3.87]) signature scores, while high expression of PD-1 indicated better outcomes (0.44 [0.21-0.94]) (Fig. 8c).

Together, these findings highlight that selected baseline NanoString signatures carry prognostic value beyond short-term treatment response and may aid in identifying patients at risk for long-term recurrence.

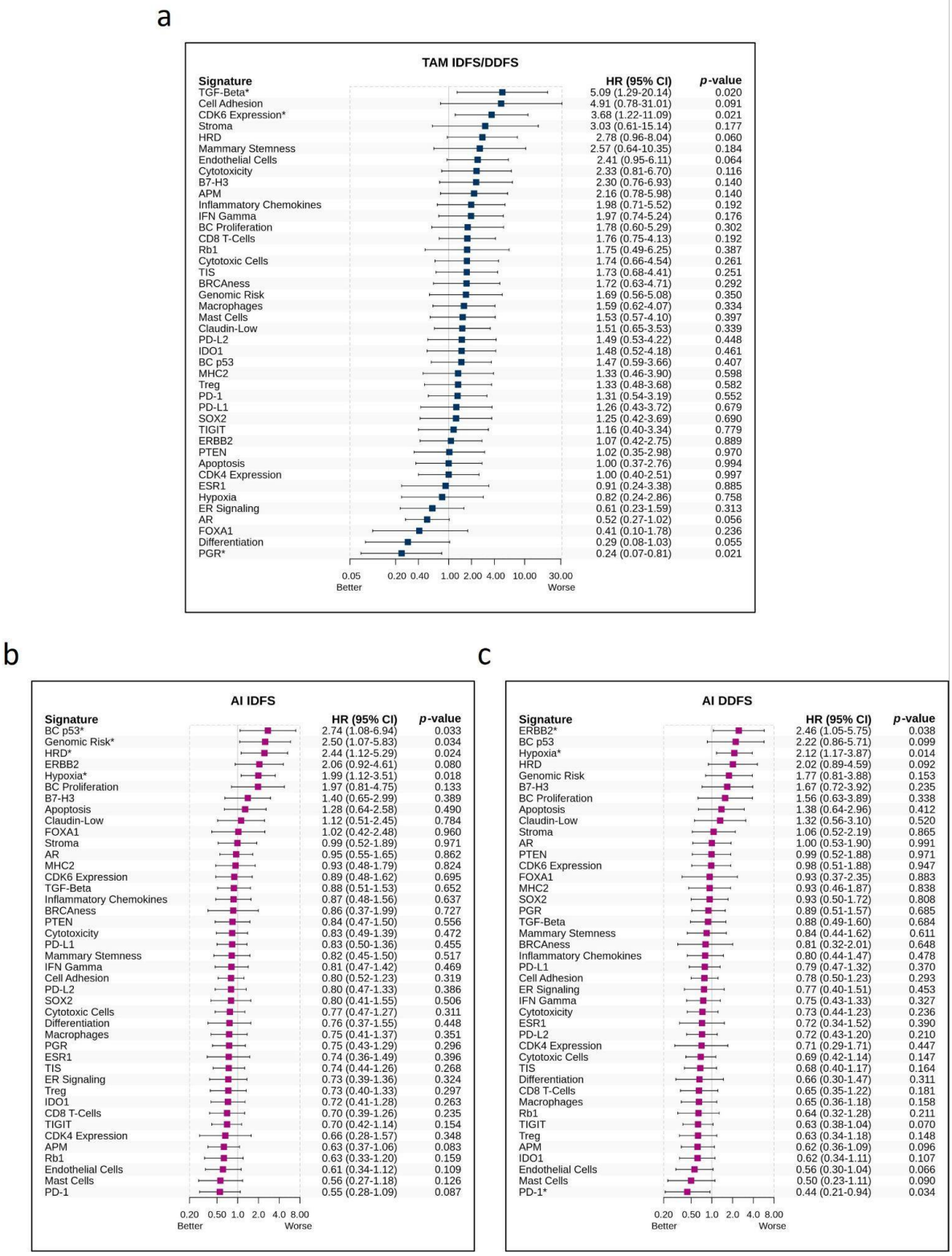

Fig 8. Associations between NanoString gene expression signatures and disease-free survival.

Association of NanoString gene expression signatures with survival endpoints (a, b) invasive disease-free survival (IDFS) and (a, c) distant disease-free survival (DDFS) in the TAM (a)

and AI cohort (b, c) were estimated by Cox regression and expressed as hazard ratios (HR) with 95% confidence intervals (95% CI) and *p*-values. In the TAM cohort (n = 125), 4 events occurred for both IDFS and DDFS; in the AI cohort (n = 66), 9 IDFS and 8 DDFS events were recorded. Median follow-up duration was 59.8 months.

Discussion

Understanding the mechanisms underlying endocrine therapy resistance in ER-positive, HER2-negative breast cancer remains a major clinical challenge. Although endocrine therapies such as tamoxifen and aromatase inhibitors are effective for many patients, a substantial proportion develop resistance, leading to recurrence and poorer outcomes. In this study, we applied an integrative approach combining transcriptomic, genomic, and clinicopathological features to identify baseline molecular correlates of endocrine response and long-term survival. Our exploratory findings provide insights into the heterogeneous nature of endocrine resistance and suggest a multifaceted biological basis for improved biomarker development and patient stratification.

Clinicopathologic analysis revealed significant age and PAM50 luminal subtype differences between responders and non-responders (Fig. 1), consistent with earlier studies linking Luminal A subtype with older age to better endocrine sensitivity [19,20]. Signature-level profiling of baseline expression showed higher variability in the AI cohort (Supplementary Fig. S2), suggesting greater biological heterogeneity, which may contribute to reduced discrimination between response groups (Fig. 7b).

Correlation analyses between gene expression and clinical features highlighted several robust associations (Fig. 2). We observed a strong negative correlation between the Luminal A PAM50 subtype correlation and proliferation-related Block C signatures (Genomic Risk, BC proliferation, and BC p53 signatures), which are significantly elevated in the non-responder group (Fig. 7a, 7b). This supports the

established understanding that tumors exhibiting higher Luminal A characteristics and inherently low proliferation rates at baseline are associated with greater endocrine responsiveness [21]. We also observed a negative correlation between differentiation signatures, reactive microenvironment and CDK6 signature scores (Block A) in endocrine therapy non-responders of the AI group (Fig. 7b) and association with worse survival outcome in the TAM group (Fig. 8a), suggesting that dedifferentiated tumors within an activated microenvironment are prone to therapy resistance. Previous studies have linked loss of differentiation to endocrine resistance [22], while a reactive stroma and immune infiltration have been shown to promote resistance through paracrine signaling [23]. Elevated CDK6 can likely bypass the growth inhibitory effects of endocrine therapy [24]. This highlights the complex interplay between intrinsic tumor properties (differentiation state) and extrinsic factors (microenvironment) in dictating therapeutic response.

Genomic profiling of post-pET tumors identified several recurrent genomic alterations (Fig. 3a). While overall RGA frequency was modest, genes such as *BRCA2*, *TP53*, *ESR1*, *CCND1*, *RB1* and *FGFR2* were more frequently altered in non-responders. Expression analyses further supported the functional relevance of these RGAs. For example, *TP53* truncating mutations were associated with significantly reduced *TP53* mRNA levels (Fig. 3f). Both *TP53* missense and truncating mutations were strongly correlated with higher immune and proliferation related signature expression (Fig. 4). These findings are in line with recent work showing that *TP53* mutations correlate with high p53 protein levels and resistance to endocrine therapy in luminal breast cancer [16,17]. *CCND1* amplification, more frequently observed in non-responders, indicated a potential mechanism of resistance through deregulated cell cycle progression, overriding the growth-inhibitory effects of endocrine therapy [25]. Notably, some of the

most frequent RGAs, e.g., *PIK3CA*, *GATA3* and *MAP3K1*, known prevalent in ER+ breast cancer [26], did not associate with resistance (Fig. 3a), but with NanoString signature scores (Fig. 4). These findings suggest that their mere presence might not be sufficient to dictate endocrine resistance in this specific context.

Integrative Factor Analysis of Mixed Data (FAMD) (Fig. 5, Fig. 6) revealed that several factors significantly contributed to patient stratification of endocrine resistance. Specifically, immune-related signatures from Block B, including the Tumor Inflammation Signature (TIS), PD-L2 expression, and TIGIT levels, alongside proliferation, genomic risk, and BC p53 signatures from Block C, emerged as key discriminators. Furthermore, specific RGAs such as *TP53*, *FGFR2*, and *CCND1* played a substantial role in this stratification. This emphasizes that combining genomic and transcriptomic data offers a deeper understanding of endocrine resistance, in contrast to using clinical markers or single assays alone.

Differential signatures expression analysis (Fig. 7a) reinforced the significant role of proliferation and immune-related programs within the TAM cohort, where non-responders exhibited higher expression of signatures such as BC Proliferation, Genomic Risk, Antigen Processing Machinery (APM), IFN Gamma signaling, and Treg (Regulatory T-cells). This aligns with studies showing that high proliferation [27] and specific immune profiles [28] can be associated with tamoxifen resistance. Interestingly, the AI cohort displayed fewer significant signature expression differences (Fig. 7b), which may stem from both biological factors, such as a more heterogeneous resistance mechanism [29] within this group, and statistical limitations due to sample size or the magnitude of gene expression changes. The observed broader transcriptomic variability in the AI cohort could also mask consistent resistance signatures across all non-responders within that group.

When stratifying the patients by RS in four risk groups, significantly differentially expressed signatures were again enriched for proliferation- and genomic risk- as well as immune-related signatures (Supplementary Fig. 6). Notably, in the RS1 group, endocrine therapy resistance was linked with elevated ER signaling. This might be an indication for estrogen-independent ER activation resulting from crosstalk with other signaling pathways [30]. We observed higher expression of Mast cell and Mammary Stemness signatures in younger, intermediate risk patients in group RS2.1. Mast cells are part of the innate immune system and were shown to promote tumor stem-like features and aggressiveness of human breast cancer [31]. In preclinical mouse models, mast cell presence has been associated with increased aggressiveness in luminal B models [32]. Consistently, we detected more LumB subtype in RS2.1 non-responders than in responders (Supplementary Fig. 5c).

The gene-level differential expression analysis (Supplementary Fig. S7) provided further granularity to the signature-level findings. In the TAM cohort, the significant upregulation of genes implicated in immune signaling and tumor-immune interaction, such as *COL11A1*, *ISG15*, *OAS3*, *CCL8*, and *CXCL10* in non-responders, reinforces the notion of a complex immune involvement in tamoxifen resistance. Overexpression of *COL11A1* has recently been reported to be associated with poor tamoxifen response [33]. The interferon-stimulated genes (*ISG15, OAS3*) and chemokines (*CCL8, CXCL10*) are known to modulate immune cell recruitment and activity within the tumor microenvironment. *ISG15* has been shown to promote tumor progression by inducing M2-like polarization of macrophages, which are associated with immunosuppressive functions [34]. The overexpression of *CXCL10* is associated with inflammation and has been linked to tumor progression and poor prognosis in breast cancer [35]. The concurrent upregulation of gene *ARNT2* associated with cellular

response to hypoxia in TAM non-responders suggests that adaptation to low oxygen conditions might also contribute to resistance, potentially by promoting angiogenesis, metabolic reprogramming, and a more aggressive phenotype [36].

In contrast, the AI cohort exhibited fewer statistically significant gene-level changes, mirroring the signature-level findings. The notable upregulation of *B3GNT3*, *NFKBIZ*, *TMPRSS4* and *SMC1B* mRNA in AI non-responders offers potential insights into resistance mechanisms. The beta-1,3-N-acetylglucosaminyltransferase *B3GNT3* has been associated with immune infiltration and activation of NF-κB pathway in several gynecologic cancers [37]. IκBζ (encoded by *NFKBIZ*) is a central inflammatory regulator of NF-κB signaling and was found upregulated in the tumor microenvironment and in association with hypoxia [38]. The increased expression of *TMPRSS4,* a serine protease involved in cell growth and invasion, and *SMC1B,* a component of the cohesin complex involved in DNA repair and chromosome segregation, links tumor proliferation and genomic instability with resistance in the AI cohort [39,40].

The analysis of baseline transcriptional profiles in relation to long-term outcomes (IDFS and DDFS) revealed distinct prognostic associations within the TAM and AI cohorts (Fig. 8). In the TAM cohort, despite limited recurrence events (n=4), higher baseline expression of TGF-Beta and CDK6 signatures suggested worse IDFS and DDFS. Conversely, higher PGR signature expression correlated with improved survival. In a previous study on 97 premenopausal patients with luminal breast cancer, we discovered the PGR signature score as a prognostic marker for a lower risk of developing distant metastases [41]. In the randomized SBII:2 trial on 236 premenopausal patients with ER+/HER2− breast cancer receiving two years of adjuvant tamoxifen treatment, NanoString gene expression signatures were measured

to evaluate long-term benefit from tamoxifen. After a median follow-up of 28 years, low signature scores for *AR*, *FOXA1,* BC Proliferation and HRD in the tamoxifen-treated group as well as high Inflammatory Chemokine scores were linked to significantly reduced risk of recurrence (adjusted hazard ratios = 0.36-0.38) [18]. Notably, our short-term resistance analysis in the TAM cohort showed non-responders exhibited higher expression of BC Proliferation, Genomic Risk, APM, IFN Gamma, and Treg signatures, aligning with the observed trends towards worse long-term outcomes associated with proliferative and certain immune-related profiles. Furthermore, the higher frequency of RGAs in *BRCA2* and *CCND1* in TAM non-responders could contribute to this aggressive phenotype and eventual recurrence [42].

In the AI cohort, the signatures showed more power for survival prediction due to more recurrence events compared to the TAM cohort. Elevated baseline scores for BC p53, Genomic Risk, HRD, and Hypoxia signatures were associated with worse IDFS. For DDFS, higher ERBB2 and Hypoxia signature scores predicted poor survival. Our short-term resistance analysis in the AI cohort indicated a weak trend towards higher CDK6 scores, and more pronounced higher expression of BC p53 and Genomic Risk in non-responders, partially mirroring the long-term prognostic associations of these signatures with poorer IDFS. Additionally, the higher frequency of recurrent genomic alterations in *ESR1*, *FGFR2*, *RB1*, and *TP53* observed in AI non-responders may contribute modestly to early resistance but appear more strongly associated with mechanisms underlying subsequent disease recurrence. A recent study on early-stage ER+ breast cancer patients treated with endocrine therapy ± radio- or chemotherapy compared mRNA expression profiles in 14 cases with local or distant recurrence (median follow-up duration 68 months) vs. 65 non-recurrent cases, using a custom NanoString nCounter panel including 145 unique genes (128 endogenous

and 17 housekeeping genes) [43]. This study identified *EZH2*, *WNT11*, *ITGB6*, and *TOP2A* as significantly upregulated in samples from recurrent cases, whereas expression of *SNAI1, ITPR1, CD10, PTEN, VDR,* and *WNT5A* were significantly downregulated. *EZH2, CD10* and *VRD* were not included in our panel. None of the remaining genes was significantly altered in our cohorts' comparing response to short-term endocrine therapy.

Our study has limitations that should be considered when interpreting the findings. The cohort size, although prospectively defined and clinically annotated, is relatively modest for survival analysis in the TAM cohort with relatively young patients. The statistical approach is explorative and hypothesis generating. Besides, the NanoString BC360 panel, while enriched for breast cancer relevant biology, covers a limited number of genes and may not capture the full complexity of endocrine resistance. Nevertheless, the ADAPT trial is a worldwide unique phase III trial allowing analysis of factors impacting on endocrine sensitivity in a cohort of pre- and postmenopausal patients receiving either tamoxifen or AI in HR+ HER2- early breast cancer [6].

Conclusions

This study provides a comprehensive integrative and explorative_analysis of transcriptomic, genomic, and clinicopathological features associated with short-term endocrine therapy response and long-term prognosis in ER-positive, HER2-negative early breast cancer. By leveraging short-term endocrine response data from a clinically annotated unique trial cohort, we demonstrate that distinct baseline molecular profiles, particularly involving immune activation, proliferation, tumor differentiation, and specific recurrent genomic alterations, are predictive of endocrine resistance.

Key findings of our hypothesis generating approach include the association of high proliferation and immune-related gene signature expression with TAM resistance, and the enrichment of genomic alterations in *TP53*, *CCND1*, *FGFR2*, and *ESR1* among non-responders. These alterations were not only more frequent in resistant tumors but also reflected functional consequences at the transcriptomic level.

Our explorative results underscore the importance of combining transcriptomic and genomic information for improved patient stratification and suggest that early transcriptional and mutational signatures may inform both therapy selection and long-term outcome predictions. These insights could be validated in future projects to support efforts to develop more personalized endocrine therapy strategies and lay the foundation for integrating multi-omic biomarkers into clinical decision-making for early-stage ER-positive breast cancer.

List of abbreviations

ADAPT, adjuvant dynamic marker-adjusted personalized therapy

AI, aromatase inhibitors

APM, Antigen processing machinery

BC, breast cancer

BC360, NanoString Breast Cancer 360™ Gene Expression Panel

CI, Confidence Interval

DDFS, distant disease-free survival

ER, estrogen receptor

ET, endocrine therapy

FAMD, factor analysis of mixed data

FDR, false discovery rate

FFPE, formalin-fixed paraffin-embedded

HER2, human epidermal growth factor receptor 2 (official name: ERBB2)

HR, hazard ratio

HRD, homologous recombination deficiency

IDFS, invasive disease-free survival

IHC, immunohistochemistry

ILBC, intralobular breast cancer

IQR, interquartile range

Ki67, proliferation marker Ki67

MHC, major histocompatibility complex

NGS, next-generation sequencing

NR, non-responder

PERCI, Predictive Endocrine ResistanCe Index

pET, preoperative endocrine therapy

PGR, progesterone receptor

pN, pathologic lymph node status

PR, progesterone receptor

pT, pathologic tumor stage

R, responder

RGA, recurrent genomic alteration

ROR, Risk of Recurrence

RS, Oncotype DX Recurrence Score

TAM, tamoxifen

TILs, tumor-infiltrating lymphocytes

TIS, tumor inflammation signatures

TP53, tumor suppressor protein p53

WSG, West German Study Group

Ethics approval and consent to participate

The study design is following the guidelines of the local ethics committee (Ethics committee of the Medical School Hannover, ID 2716-2015). Written consent was obtained by the participants.

Consent for publication

Not applicable.

Availability of data and materials

The NanoString RNA expression dataset supporting the conclusions of this article is available in the GEO repository [GSE277607: https://www.ncbi.nlm.nih.gov/geo/query/acc.cgi?acc=GSE277607]. The NGS panel sequencing data is available in the EGA repository [xxx: https://xxx].

Access to survival data from the WSG-ADAPT trial is restricted.

Competing interests

O.G. and N.H. have minority ownership interest in WSG GmbH; O.G. received honoraria from Genomic Health/Exact Sciences, Roche, Celgene, Pfizer, Novartis, NanoString Technologies, and AstraZeneca; served in consulting/advisory role for Celgene, Genomic Health/Exact Sciences, Lilly, MSD, Novartis, Pfizer, and Roche; and received travel support from Roche. N.H. received honoraria from Amgen, AstraZeneca, Genomic Health, Novartis, Pfizer, Pierre Fabre, Roche, and Zodiac Pharma; served in consulting/advisory role for Agendia, AstraZeneca, Celgene, Daiichi Sankyo, Lilly, Merck Sharp & Dohme, Novartis, Odonate Therapeutics, Pfizer, Pierre Fabre, Roche/Genentech, Sandoz, and Seattle Genetics; her institution received research funding from Lilly, Merck Sharp & Dohme, Novartis, Pfizer, and

Roche/Genentech. R.K. served in a consulting/advisory role for the West German Study Group.

Funding

The study was supported by a grant from the German Cancer Aid (Deutsche Krebshilfe) Grant Number 70112954. G.Z. was financed by DIFUTURE Grant Number BMBF 01ZZ1804C. H.N. received a scholarship form the China Scholarship Council (CSC) (Number: 201806010411). The funding body had no role in the design, data analysis, or manuscript preparation/publication.

Authors' contributions

H.K., N.H. and M.C. designed the study. O.G., M.G., S.K., U.N. and N.H. collected patient samples and data. R.K. and M.C. selected the patients and performed the matching. M.C., H.C., L.D.K. and M.R. performed the immunohistochemical stainings and pathology assessment. S.B., G.Z., C.G., U.M., L.M., C.zE. and H.N. performed the experiments, analyzed, and interpreted the data. U.M. provided supervision. G.Z. and C.G. wrote the manuscript. H.K., C.P., N.H. and U.M. reviewed and edited the manuscript. All authors read and approved the final manuscript.

Acknowledgements

We thank the patients and families who contributed to this study.

References

1. Hanker AB, Sudhan DR, Arteaga CL. Overcoming Endocrine Resistance in Breast Cancer. Cancer Cell. 2020;37: 496–513. doi:10.1016/j.ccell.2020.03.009

2. Spring LM, Gupta A, Reynolds KL, Gadd MA, Ellisen LW, Isakoff SJ, et al. Neoadjuvant endocrine therapy for estrogen receptor-positive breast cancer: A systematic review and meta-analysis. JAMA Oncol. 2016;2: 1477–1486. doi:10.1001/jamaoncol.2016.1897

3. Normanno N, Di Maio M, De Maio E, De Luca A, de Matteis A, Giordano A, et

al. Mechanisms of endocrine resistance and novel therapeutic strategies in breast cancer. Endocr Relat Cancer. 2005;12: 721–747. doi:10.1677/erc.1.00857

4. Hartkopf AD, Grischke E-M, Brucker SY. Endocrine-resistant breast cancer: Mechanisms and treatment. Breast Care (Basel). 2020;15: 347–354. doi:10.1159/000508675

5. Will M, Liang J, Metcalfe C, Chandarlapaty S. Therapeutic resistance to anti-oestrogen therapy in breast cancer. Nat Rev Cancer. 2023;23: 673–685. doi:10.1038/s41568-023-00604-3

6. Nitz UA, Gluz O, Kummel S, Christgen M, Braun M, Aktas B, et al. Endocrine Therapy Response and 21-Gene Expression Assay for Therapy Guidance in HR+/HER2- Early Breast Cancer. J Clin Oncol. 2022;40: 2557–2567. doi:10.1200/JCO.21.02759

7. Harvell DME, Spoelstra NS, Singh M, McManaman JL, Finlayson C, Phang T, et al. Molecular signatures of neoadjuvant endocrine therapy for breast cancer: characteristics of response or intrinsic resistance. Breast Cancer Res Treat. 2008;112: 475–488. doi:10.1007/s10549-008-9897-4

8. Goto-Yamaguchi L, Yamamoto-Ibusuki M, Yamamoto Y, Fujiki Y, Tomiguchi M, Sueta A, et al. Therapeutic predictors of neoadjuvant endocrine therapy response in estrogen receptor-positive breast cancer with reference to optimal gene expression profiling. Breast Cancer Res Treat. 2018;172: 353–362. doi:10.1007/s10549-018-4933-5

9. NCounter® Breast Cancer 360™. In: NanoString [Internet]. NanoString Technologies, Inc.; 2 Dec 2020 [cited 28 Mar 2025]. Available: https://nanostring.com/products/ncounter-assays-panels/oncology/breast-cancer-360/

10. Paik S, Shak S, Tang G, Kim C, Baker J, Cronin M, et al. A multigene assay to predict recurrence of tamoxifen-treated, node-negative breast cancer. N Engl J Med. 2004;351: 2817–2826. doi:10.1056/NEJMoa041588

11. Cobleigh MA, Tabesh B, Bitterman P, Baker J, Cronin M, Liu M-L, et al. Tumor gene expression and prognosis in breast cancer patients with 10 or more positive lymph nodes. Clin Cancer Res. 2005;11: 8623–8631. doi:10.1158/1078-0432.CCR-05-0735

12. Zhang G, Jurinovic V, Bartels S, Christgen M, Christgen H, Kandt LD, et al. Development and validation of multivariate predictors of primary endocrine resistance to tamoxifen and aromatase inhibitors in luminal breast cancer reveal drug-specific differences. medRxiv. 2023. p. 2023.11.13.23298466. doi:10.1101/2023.11.13.23298466

13. Graeser M, Gluz O, Biehl C, Ulbrich-Gebauer D, Christgen M, Palatty J, et al. Impact of RNA signatures on pCR and survival after 12-week neoadjuvant pertuzumab plus trastuzumab with or without paclitaxel in the WSG-ADAPT

HER2+/HR- trial. Clin Cancer Res. 2023;29: 805–814. doi:10.1158/1078-0432.CCR-22-1587

14. Wallden B, Storhoff J, Nielsen T, Dowidar N, Schaper C, Ferree S, et al. Development and verification of the PAM50-based Prosigna breast cancer gene signature assay. BMC Med Genomics. 2015;8: 54. doi:10.1186/s12920-015-0129-6

15. Lê S, Josse J, Husson F. FactoMineR: AnRPackage for Multivariate Analysis. J Stat Softw. 2008;25. doi:10.18637/jss.v025.i01

16. Mueller S, Grote I, Bartels S, Kandt L, Christgen H, Lehmann U, et al. P53 expression in luminal breast cancer correlates with TP53 mutation and primary endocrine resistance. Mod Pathol. 2023;36: 100100. doi:10.1016/j.modpat.2023.100100

17. Grote I, Bartels S, Kandt L, Bollmann L, Christgen H, Gronewold M, et al. TP53 mutations are associated with primary endocrine resistance in luminal early breast cancer. Cancer Med. 2021;10: 8581–8594. doi:10.1002/cam4.4376

18. Lundgren C, Tutzauer J, Church SE, Stål O, Ekholm M, Forsare C, et al. Tamoxifen-predictive value of gene expression signatures in premenopausal breast cancer: data from the randomized SBII:2 trial. Breast Cancer Res. 2023;25: 110. doi:10.1186/s13058-023-01719-z

19. Lian W, Fu F, Lin Y, Lu M, Chen B, Yang P, et al. The impact of young age for prognosis by subtype in women with early breast cancer. Sci Rep. 2017;7: 11625. doi:10.1038/s41598-017-10414-x

20. Gao JJ, Swain SM. Luminal A breast cancer and molecular assays: A review. Oncologist. 2018;23: 556–565. doi:10.1634/theoncologist.2017-0535

21. Xiong X, Zheng L-W, Ding Y, Chen Y-F, Cai Y-W, Wang L-P, et al. Breast cancer: pathogenesis and treatments. Signal Transduct Target Ther. 2025;10: 49. doi:10.1038/s41392-024-02108-4

22. Kim MR, Wu M-J, Zhang Y, Yang J-Y, Chang CJ. TET2 directs mammary luminal cell differentiation and endocrine response. Nat Commun. 2020;11: 4642. doi:10.1038/s41467-020-18129-w

23. Feng B, Wu J, Shen B, Jiang F, Feng J. Cancer-associated fibroblasts and resistance to anticancer therapies: status, mechanisms, and countermeasures. Cancer Cell Int. 2022;22: 166. doi:10.1186/s12935-022-02599-7

24. Wang X, Zhao S, Xin Q, Zhang Y, Wang K, Li M. Recent progress of CDK4/6 inhibitors' current practice in breast cancer. Cancer Gene Ther. 2024;31: 1283–1291. doi:10.1038/s41417-024-00747-x

25. Hanf D, Fasching P, Gass P, Matthias W Beckmann, Hack CC, Heindl F, et al. Impact of CCND1 amplification on the prognosis of hormone receptor-positive, HER2-negative breast cancer patients-correlation of clinical and pathological markers. Breast Cancer Res Treat. 2025;210: 125–134. doi:10.1007/s10549-

024-07545-x

26. Schagerholm C, Robertson S, Toosi H, Sifakis EG, Hartman J. PIK3CA mutations in endocrine-resistant breast cancer. Sci Rep. 2024;14: 12542. doi:10.1038/s41598-024-62664-1

27. Zhu J, Ye L, Sun S, Yuan J, Huang J, Zeng Z. Involvement of RFC3 in tamoxifen resistance in ER-positive breast cancer through the cell cycle. Aging (Albany NY). 2023;15: 13738–13752. doi:10.18632/aging.205260

28. Kastrati I, Joosten SEP, Semina SE, Alejo LH, Brovkovych SD, Stender JD, et al. The NF-κB pathway promotes tamoxifen tolerance and disease recurrence in estrogen receptor-positive breast cancers. Mol Cancer Res. 2020;18: 1018–1027. doi:10.1158/1541-7786.MCR-19-1082

29. Ma CX, Reinert T, Chmielewska I, Ellis MJ. Mechanisms of aromatase inhibitor resistance. Nat Rev Cancer. 2015;15: 261–275. doi:10.1038/nrc3920

30. Musheyev D, Alayev A. Endocrine therapy resistance: what we know and future directions. Explor Target Antitumor Ther. 2022;3: 480–496. doi:10.37349/etat.2022.00096

31. Bongiorno R, Lecchi M, Botti L, Bosco O, Ratti C, Fontanella E, et al. Mast cell heparanase promotes breast cancer stem-like features via MUC1/estrogen receptor axis. Cell Death Dis. 2024;15: 709. doi:10.1038/s41419-024-07092-9

32. Majorini MT, Colombo MP, Lecis D. Few, but efficient: The role of mast cells in breast cancer and other solid tumors. Cancer Res. 2022;82: 1439–1447. doi:10.1158/0008-5472.CAN-21-3424

33. Fu C, Duan S, Zhou X, Meng Y, Chen X. Overexpression of COL11A1 confers tamoxifen resistance in breast cancer. NPJ Breast Cancer. 2024;10: 38. doi:10.1038/s41523-024-00645-3

34. Chen R-H, Xiao Z-W, Yan X-Q, Han P, Liang F-Y, Wang J-Y, et al. Tumor cell-secreted ISG15 promotes tumor cell migration and immune suppression by inducing the macrophage M2-like phenotype. Front Immunol. 2020;11: 594775. doi:10.3389/fimmu.2020.594775

35. Kim M, Choi HY, Woo JW, Chung YR, Park SY. Role of CXCL10 in the progression of in situ to invasive carcinoma of the breast. Sci Rep. 2021;11: 18007. doi:10.1038/s41598-021-97390-5

36. Morotti M, Bridges E, Valli A, Choudhry H, Sheldon H, Wigfield S, et al. Hypoxia-induced switch in SNAT2/SLC38A2 regulation generates endocrine resistance in breast cancer. Proc Natl Acad Sci U S A. 2019;116: 12452–12461. doi:10.1073/pnas.1818521116

37. Xu J, Guo Z, Yuan S, Li H, Luo S. Upregulation of B3GNT3 is associated with immune infiltration and activation of NF-κB pathway in gynecologic cancers. J Reprod Immunol. 2022;152: 103658. doi:10.1016/j.jri.2022.103658

38. Feng Y, Chen Z, Xu Y, Han Y, Jia X, Wang Z, et al. The central inflammatory regulator IκBζ: induction, regulation and physiological functions. Front Immunol. 2023;14: 1188253. doi:10.3389/fimmu.2023.1188253

39. Li X-M, Liu W-L, Chen X, Wang Y-W, Shi D-B, Zhang H, et al. Overexpression of TMPRSS4 promotes tumor proliferation and aggressiveness in breast cancer. Int J Mol Med. 2017;39: 927–935. doi:10.3892/ijmm.2017.2893

40. Ibrahim A, Toss MS, Alsaleem M, Makhlouf S, Atallah N, Green AR, et al. Novel 2 gene signatures associated with breast cancer proliferation: Insights from predictive differential gene expression analysis. Mod Pathol. 2024;37: 100403. doi:10.1016/j.modpat.2023.100403

41. Ni H, Kumbrink J, Mayr D, Seiler A, Hagemann F, Degenhardt T, et al. Molecular prognostic factors for distant metastases in premenopausal patients with HR+/HER2- early Breast Cancer. J Pers Med. 2021;11: 835. doi:10.3390/jpm11090835

42. Nebenfuehr S, Kollmann K, Sexl V. The role of CDK6 in cancer. Int J Cancer. 2020;147: 2988–2995. doi:10.1002/ijc.33054

43. Jones V, Yin HH, Yuan Y-C, Wang Y, Li SM, Aljaber D, et al. Gene expression associated with endocrine therapy resistance in estrogen receptor-positive breast cancer. Sci Rep. 2025;15: 7220. doi:10.1038/s41598-025-89274-9

Supplementary Figures

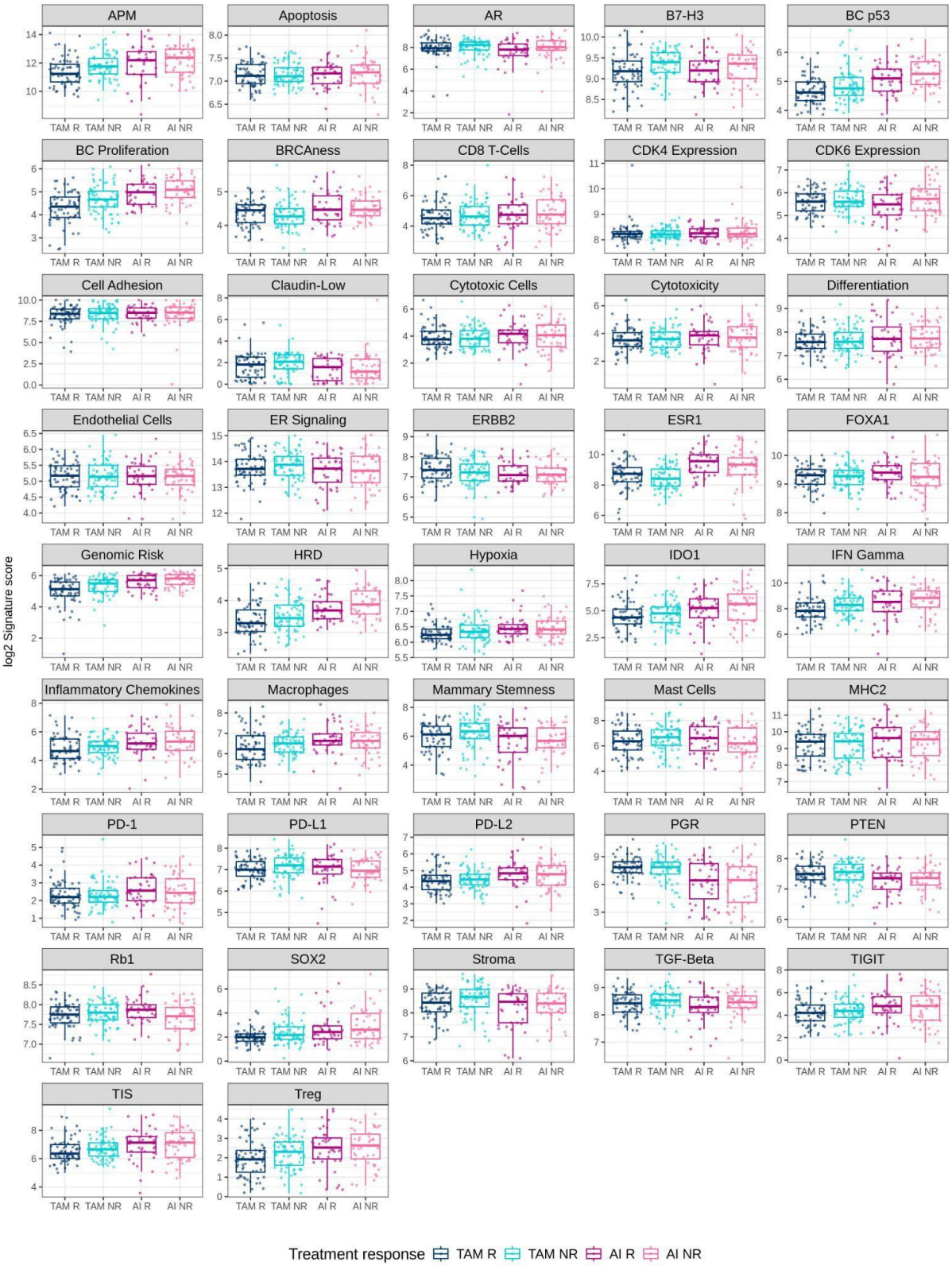

Supplementary Fig. S1: Overview of NanoString gene expression signature scores.

NanoString gene expression signature scores are stratified by treatment and response groups. Boxplots display the median (line), interquartile range (box), and whiskers extending to 1.5 times the interquartile range (IQR).

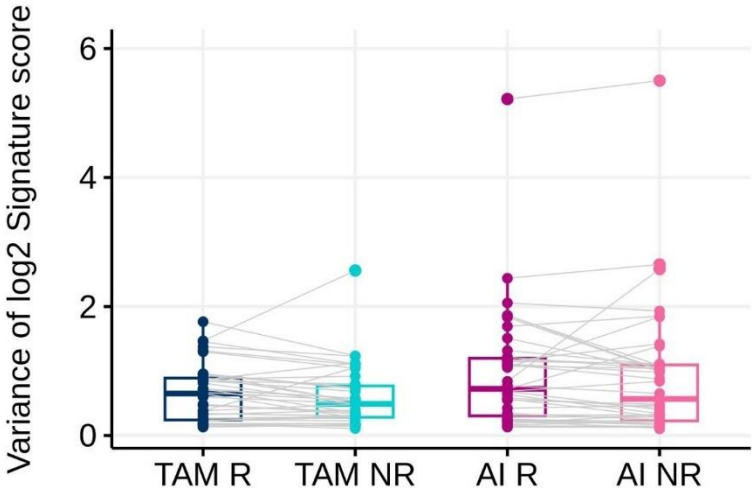

Supplementary Fig. S2: Variance of NanoString gene expression signature scores per treatment response group.

Log2-transformed NanoString BC360 signature scores were used to calculate variance within each treatment and response group. Identical signatures across groups are connected by grey lines. Boxplots display the median (line), interquartile range (box), and whiskers extending to 1.5 times the interquartile range (IQR).

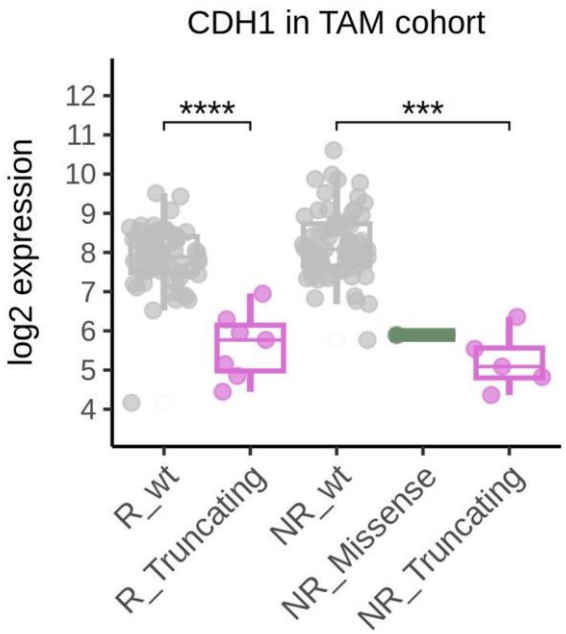

Supplementary Fig. S3: CDH1 mRNA expression in TAM cohort.

NanoString log2 mRNA expression levels of CDH1, separated by mutation types and analyzed using Wilcoxon rank sum test with ***, ****, p-value < 0.001, 0.0001. Boxplots show median (line), upper, and lower quartiles (boxes), and lines extending to 1.5-IQR (whiskers).

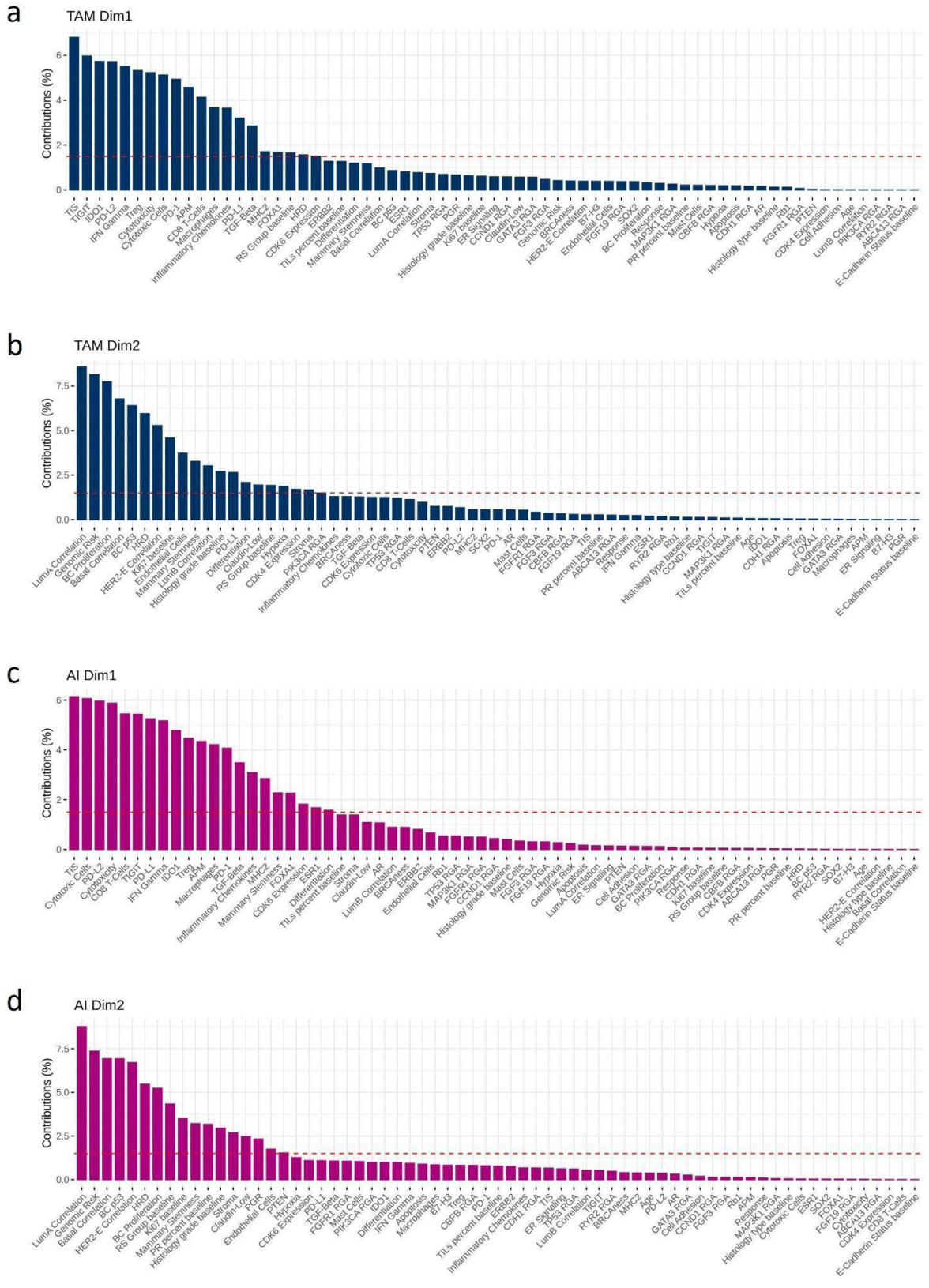
a
TAM Dim1
Contributions (%)
b
TAM Dim2
Contributions (%)
c
AI Dim1
Contributions (%)
d
AI Dim2
Contributions (%)

Supplementary Fig. S4: Summary of contributions to FAMD dimension 1 and 2.

Contributions of all signatures, clinical features and RGAs to the 1. and 2. dimensions of Factor Analysis of Mixed Data (FAMD) in TAM cohort (a, b) and AI cohort (c, d), sorted in decreasing order per dimension. Extensions “RGA” to the feature names annotates genomic alterations whereas feature names without extensions point to gene expression data. The red dashed lines indicate expected average values, if the contributions were uniform.

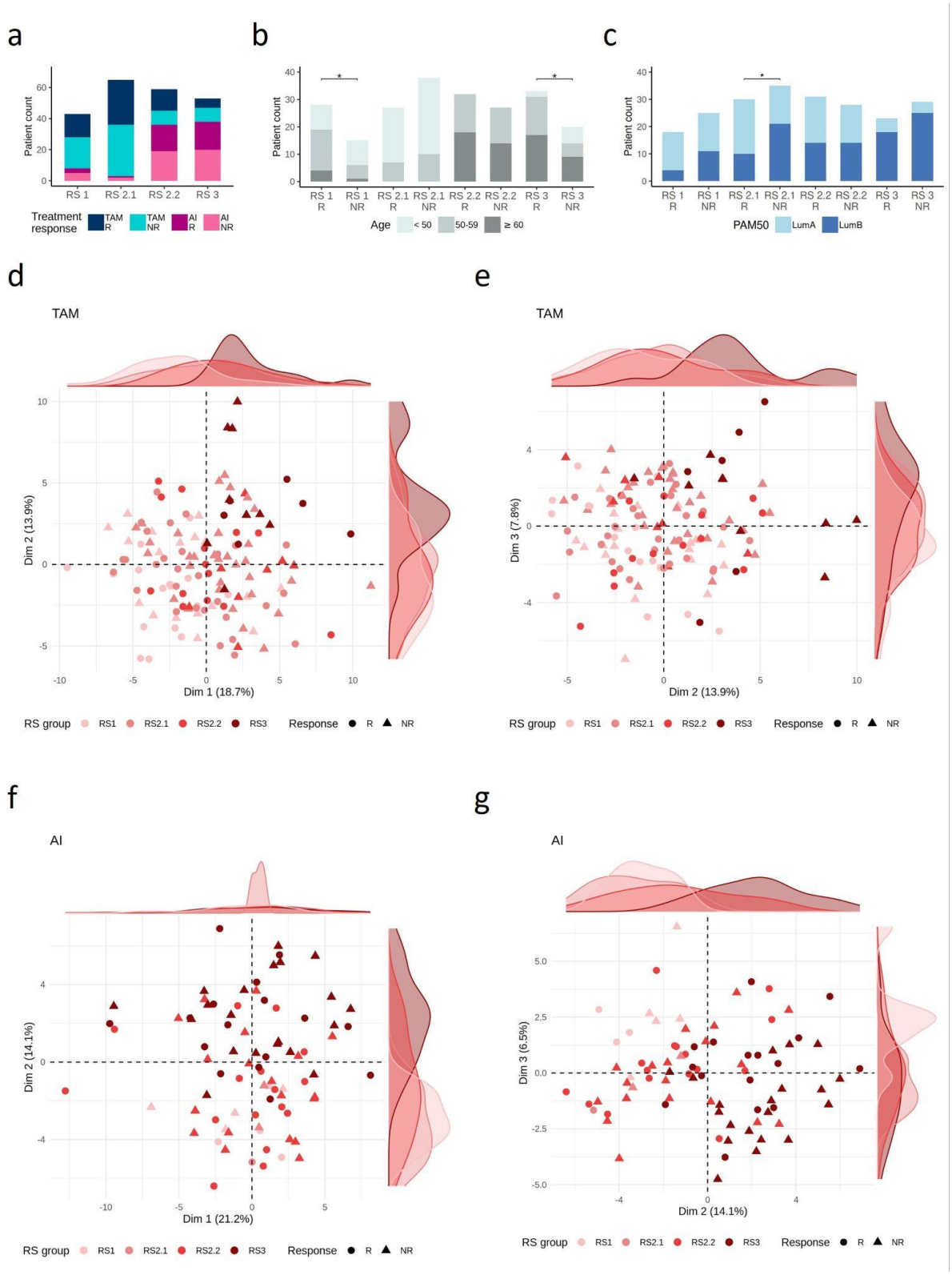

Supplementary Fig. S5. Factor analysis of mixed data (FAMD) labeled by RS risk and response groups.

Stacked barplots indicating the distribution of treatment response (a), age groups (b), and PAM50 subtypes (c) per RS response groups. Statistical analysis using Generalized Linear Mixed-Effects Models (glmer) with patient pair_id as a random effect. Asterisks * indicates *p*-

values < 0.05. Distribution of TAM cohort (c, d) and AI cohort (e, f) in Dim1 vs. Dim2 (a, c) and in Dim2 vs. Dim3 (b, d) based on their signature expression scores, RGA and clinico-pathological characteristics in a two-dimensional space using FAMD. RS risk groups are color coded, and responders (R) and non-responders (NR) are indicated by different shapes. Density curves at the outside of the plots indicate patient counts.

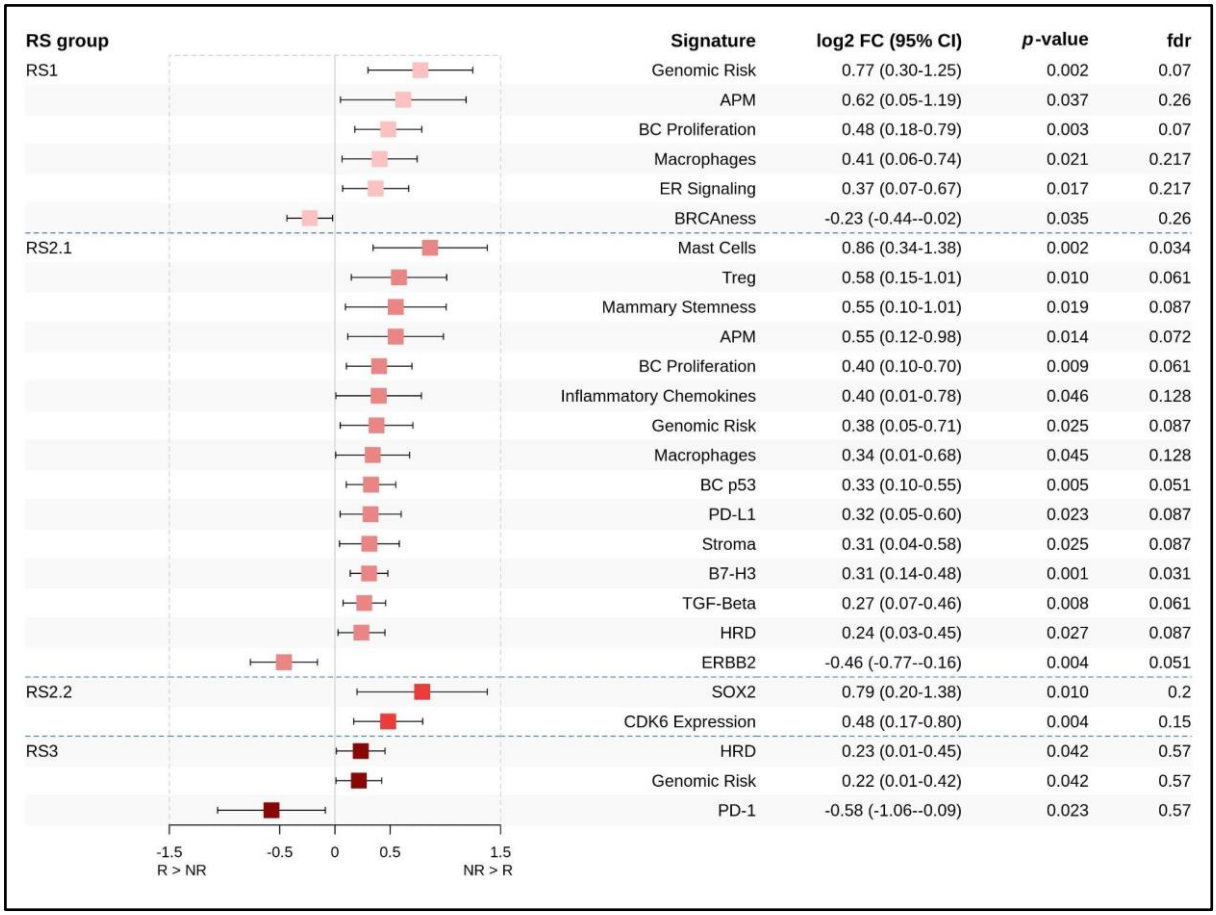

Supplementary Fig. S6. Differential expression of gene signatures between R and NR per RS risk group.

Summary of differential signature expression between response groups per RS risk group by fitting linear mixed models with patient pair_id as a random effect. The following variables are used as covariates: RS1: age; RS2.1: age and TILs group at baseline; RS3: age. Only significant signatures with *p*-values < 0.05 are shown. Signatures are sorted by log2 fold change of mean signature expression between responders and non-responders per RS risk group. 95% confidence intervals of log2 fold change, *p*-values and fdr-adjusted *p*-values are shown.

a

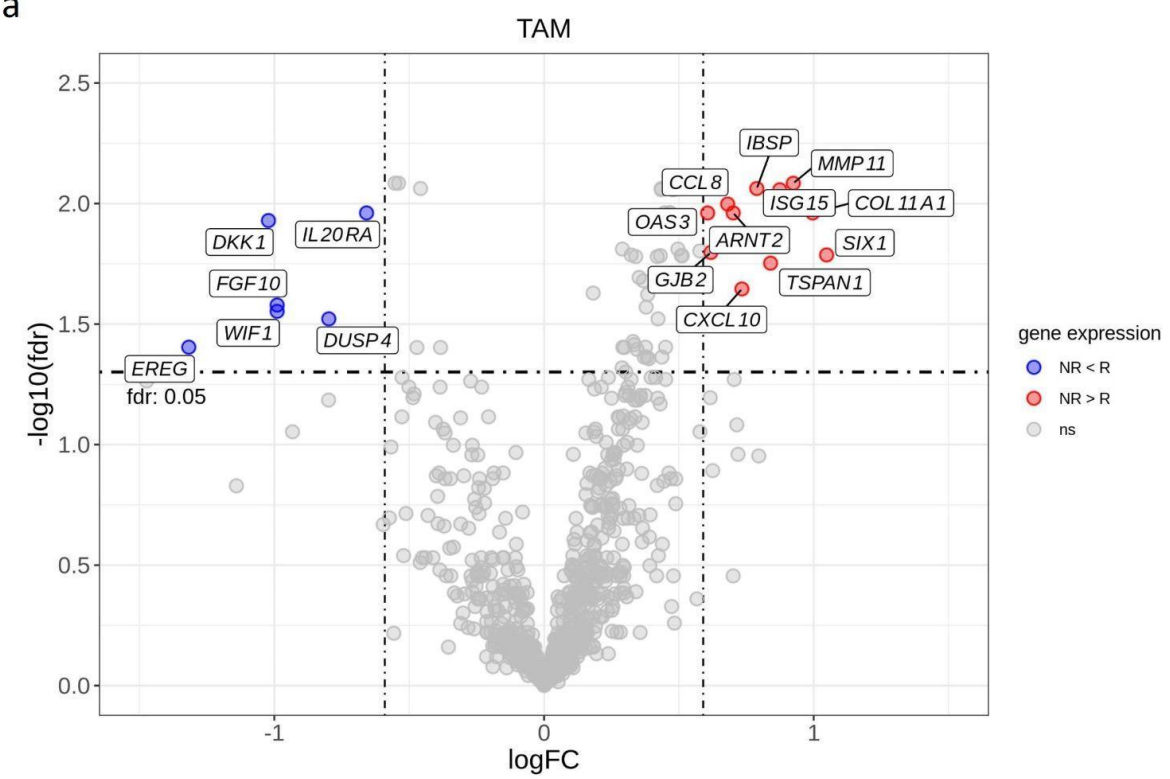
TAM
-log10(fdr)
logFC
fdr: 0.05
DKK1
IL20RA
FGF10
WIF1
DUSP4
EREG
IBSP
MMP11
CCL8
ISG15
COL11A1
OAS3
ARNT2
SIX1
GJB2
TSPAN1
CXCL10
gene expression
NR < R
NR > R
ns

b

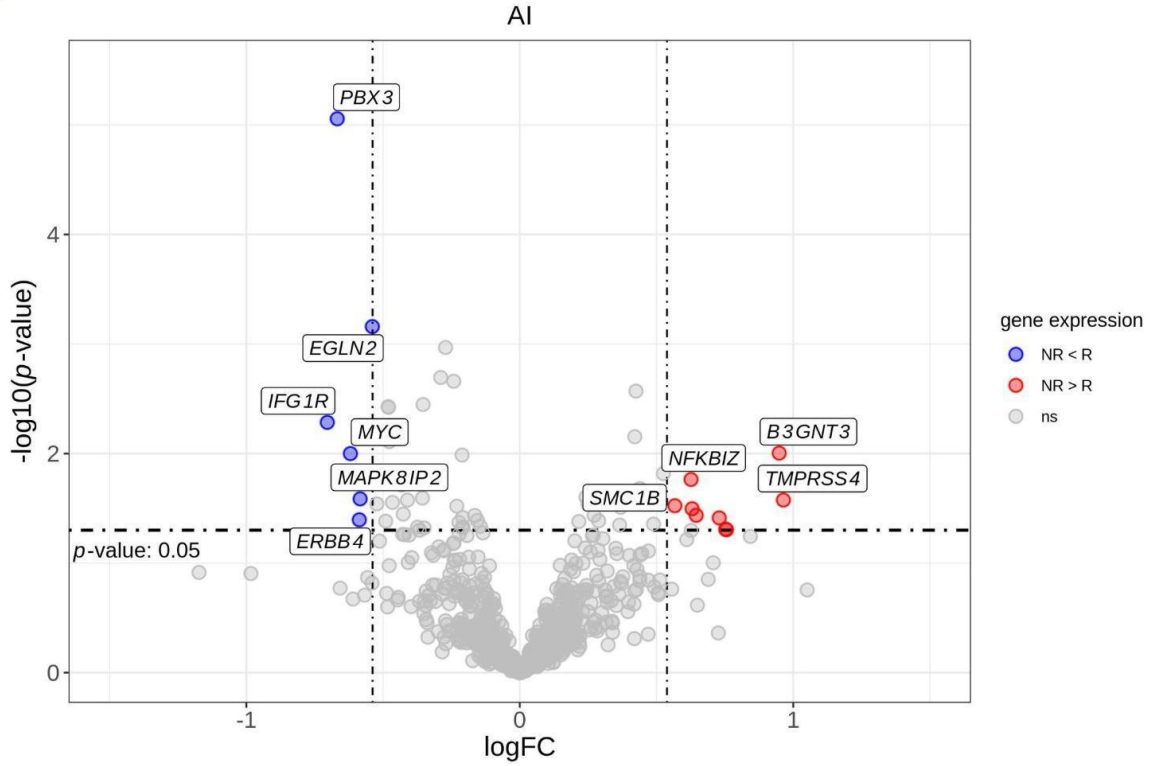
AI
-log10(p-value)
logFC
p-value: 0.05
PBX3
EGLN2
IFG1R
MYC
MAPK8IP2
ERBB4
B3GNT3
NFKBIZ
TMPRSS4
SMC1B
gene expression
NR < R
NR > R
ns

Supplementary Fig. S7: Volcano plots of differentially expressed genes between response groups.

Volcano plots of differential gene expression between response groups in the TAM (a) and AI (b) cohort by fitting linear mixed models with patient pair_id as a random effect. The following variables are used as covariates: TAM: age and TILs group at baseline; AI: age. Significantly up/down-regulated genes (cutoff: mean ± 2*sd of logFC and fdr < 0.05 in TAM cohort and *p*-value < 0.05 in AI cohort) are color coded in red and blue, respectively and labeled. The dashed horizontal line indicates the significance cutoff and the dashed vertical lines indicate the logFC cutoffs.

Supplementary Tables

Supplementary Table S1. Clinico-pathologic characteristics of the NanoString cohort

	ALL	**TAM**		**AI**			
		Responder[a]	**Non-Responder[b]**	**Responder[a]**	**Non-Responder[b]**		
	n=220	**n=64**	**n=71**	**n=39**	**n=46**	***P_{TAM}***	***P_{AI}***
	n (%)	n (%)	n (%)	n (%)	n (%)		
age						***0.024***	***0.003***
< 50	74 (34%)	31 (46%)	41 (58%)	0	2 (4%)		
50 - 59	83 (37%)	28 (44%)	29 (40%)	5 (12%)	21 (46%)		
≥ 60	63 (29%)	5 (10%)	1 (2%)	34 (88%)	23 (50%)		
histology, baseline						*0.944*	*0.929*
NST	201 (91%)	57 (89%)	62 (87%)	38 (97%)	44 (96%)		
ILBC	19 (9%)	7 (11%)	9 (13%)	1 (3%)	2 (4%)		
pT stage						*0.906*	*0.929*
pT1	141 (64%)	42 (66%)	44 (62%)	24 (62%)	31 (67%)		
pT2	78 (35%)	22 (34%)	26 (37%)	15 (38%)	15 (33%)		
pT3	1 (1%)	0	1 (1%)	0	0		
pT4	0	0	0	0	0		
pN stage						*0.988*	*0.918*
pN0	206 (94%)	61 (95%)	68 (96%)	36 (92%)	41 (89%)		
pN1+	14 (6%)	3 (5%)	3 (4%)	3 (8%)	5 (11%)		
grade, baseline						*0.893*	*0.961*
G1	11 (5%)	6 (9%)	4 (6%)	0	1 (2%)		
G2	113 (51%)	40 (63%)	47 (66%)	11 (28%)	15 (33%)		
G3	96 (44%)	18 (28%)	20 (28%)	28 (72%)	30 (65%)		
ER, baseline						*NA*	*NA*

> 10%	218 (99%)	64 (100%)	71 (100%)	38 (97%)	45 (98%)		
≤ 10%	0	0	0	0	0		
n.a.	2 (1%)	0	0	1 (3%)	1 (2%)		
PR, baseline						*0.388*	*0.202*
> 10%	188 (85%)	61 (95%)	65 (92%)	31 (79%)	31 (67%)		
≤ 10%	32 (15%)	3 (5%)	6 (8%)	8 (21%)	15 (33%)		
HER2, baseline						*0.787*	*0.540*
IHC 0/1+	193 (88%)	56 (88%)	61 (86%)	34 (87%)	42 (91%)		
IHC 2+, FISH-neg	25 (11%)	8 (12%)	9 (13%)	4 (10%)	4 (9%)		
IHC 2+, FISH-pos[c]	2 (1%)	0	1 (1%)	1 (3%)	0		
IHC 3+[c]	0	0	0	0	0		
E-cadherin, baseline						*0.165*	*0.097*
pos.	197 (89%)	55 (86%)	61 (86%)	37 (95%)	44 (96%)		
neg.	22 (10%)	9 (14%)	9 (13%)	2 (5%)	2 (4%)		
n.a.	1 (1%)	0	1 (1%)	0	0		
Ki67, baseline						*0.647*	*0.974*
0% - 9%	14 (6%)	7 (11%)	5 (7%)	1 (3%)	1 (2%)		
10% - 19%	53 (24%)	18 (28%)	21 (39%)	7 (18%)	7 (15%)		
20% - 34%	127 (58%)	34 (53%)	39 (47%)	23 (59%)	31 (68%)		
35% - 100%	26 (12%)	5 (8%)	6 (7%)	8 (20%)	7 (15%)		
Luminal Subtype[d], baseline						*0.226*	*0.963*
LumA	164 (75%)	57 (89%)	58 (82%)	22 (56%)	27 (59%)		
LumB	56 (25%)	7 (11%)	13 (18%)	17 (44%)	19 (41%)		
PAM50[e], baseline						***0.044***	*0.299*
LumA	102 (46%)	41 (64%)	33 (46%)	15 (38%)	13 (28%)		
LumB	117 (53%)	23 (36%)	38 (54%)	23 (59%)	33 (72%)		
HER2-E	1 (0%)	0	0	1 (3%)	0		
TILs[f], baseline						***0.023***[g]	*0.821*[g]

0% - 9%	160 (73%)	43 (67%)	59 (83%)	25 (64%)	33 (72%)		
10% - 40%	53 (24%)	20 (31%)	11 (15%)	11 (28%)	11 (24%)		
41% - 100%	3 (1%)	1 (2%)	0	0	2 (4%)		
n.a.	4 (2%)	0	1 (2%)	3 (8%)	0		
Oncotype DX RS Group, baseline						*0.885*	*0.914*
1 (0 -11)	43 (20%)	15 (23%)	20 (28%)	3 (8%)	5 (11%)		
2 (12 – 25)	124 (56%)	43 (67%)	42 (59%)	18 (46%)	21 (46%)		
3 (26 – 100)	55 (24%)	6 (10%)	9 (13%)	18 (46%)	20 (43%)		

Unless otherwise stated, the values are given in the format n (%), with n corresponding to the number of patients. For the statistical analysis between the Responder and Non-Responder groups, Cumulative Link Mixed Model (clmm) with patient pair_id as a random effect was used to compare Ki67 at baseline and Generalized Linear Mixed-Effects Models (glmer) with patient pair_id as a random effect were used for all other comparisons. Significant differences are highlighted in bold. “NA” indicates data with clear separation therefore the p value is not available.

n.a. not available, ER estrogen receptor, PR progesterone receptor, pET preoperative endocrine therapy, RS recurrence score, LumA Luminal A, lumB Luminal B, TAM tamoxifen, AI aromatase inhibitors.

a: Responder was defined as post-pET Ki67 < 10% and relative Ki67 decrease of ≤ -70% from baseline to post-pET.

b: Non-reponder was defined as post-pET Ki67 of ≥ 20% and relative Ki67 decrease of > -20% from baseline to post-pET.

c: HER2-positivity in a minor subclone of < 10% of tumor cells; not HER2-positive according to ASCO/CAP-Guidelines (Ref. Wolff et al. 2018).

d: Luminal B: Ki67 baseline ≥ 35% or PR baseline ≤ 20%, Luminal A: all others.

e: Intrinsic subtypes of breast cancer using PAM50 gene expression signatures.

f: Stromal tumor-infiltrating lymphocytes in pathologic tissue sections.

g: Comparison only between the first three category groups.

Supplementary Table S2. (xlsx)

Tab1. List of content

Tab2. Clinico-pathological data and PERCI

Tab3. Biological categories and block assignment of baseline NanoString gene expression signatures

Tab4. Baseline NanoString signatures and PAM50 values

Tab5. Correlation of baseline NanoString signatures with clinico-pathological parameters and PAM50 correlations in TAM group

Tab6. Correlation of baseline NanoString signatures with clinico-pathological parameters and PAM50 correlations in AI group

Tab7. Details of mutations and copy number status

Tab8. Baseline NanoString gene expression log2 values

Tab9. Association between RGA and baseline NanoString signatures (signed log10 p-adjust)

Tab10. Factor analysis of mixed data (FAMD) in TAM group

Tab11. Factor analysis of mixed data (FAMD) in AI group

Tab12. Feature contributions of FAMD in TAM group

Tab13. FAMD AI contributions Feature contributions of FAMD in AI group

Tab14. Linear mixed model results of FAMD Dimensions 1 to 3 in TAM group (R vs. NR)

Tab15. Linear mixed model results of FAMD Dimensions 1 to 3 in TAM group (RS risk groups: RS1, RS2.1, RS2.2, RS3)

Tab16. Linear mixed model results of FAMD Dimensions 1 to 3 in AI group (R vs. NR)

Tab17. Linear mixed model results of FAMD Dimensions 1 to 3 in AI group (RS risk groups: RS1, RS2.1, RS2.2, RS3)

Tab18. Differential analysis of baseline NanoString signatures between responders and non-responders in TAM group

Tab19. Differential analysis of baseline NanoString signatures between responders and non-responders in AI group

Tab20. Differential analysis of baseline NanoString signatures between responders and non-responders in RS1 group

Tab21. Differential analysis of baseline NanoString signatures between responders and non-responders in RS2 group (age ≤ 51)

Tab22. Differential analysis of baseline NanoString signatures between responders and non-responders in RS2 group (age > 51)

Tab23. Differential analysis of baseline NanoString signatures between responders and non-responders in RS3 group

Tab24. Differential analysis of baseline NanoString gene expression between responders and non-responders in TAM group

Tab25. Differential analysis of baseline NanoString gene expression between responders and non-responders in AI group